OPTOMECHANICALLY INDUCED TRANSPARENCY IN A $\mathcal{PT}$ SYMMETRIC SYSTEM

A THESIS SUBMITTED TO

THE GRADUATE SCHOOL OF ENGINEERING AND SCIENCE

OF BILKENT UNIVERSITY

IN PARTIAL FULFILLMENT OF THE REQUIREMENTS FOR

THE DEGREE OF

MASTER OF SCIENCE

IN

PHYSICS

By

Beyza Sütlüoğlu

August 2020

OPTOMECHANICALLY INDUCED TRANSPARENCY IN A $\mathcal{PT}$ SYMMETRIC SYSTEM

By Beyza Sütlüoğlu

August 2020

We certify that we have read this thesis and that in our opinion it is fully adequate, in scope and in quality, as a thesis for the degree of Master of Science.

Ceyhun Bulutay(Advisor)

Oğuz Gülseren

Cem Yüce

Approved for the Graduate School of Engineering and Science:

Ezhan Karaşan
Director of the Graduate School

ABSTRACT

OPTOMECHANICALLY INDUCED TRANSPARENCY IN A $\mathcal{PT}$ SYMMETRIC SYSTEM

Beyza Sütlüoğlu
M.S. in Physics
Advisor: Ceyhun Bulutay
August 2020

Optomechanical systems have attracted attention recently in various areas of physics, and are widely used with the purpose of laser cooling, gravitational wave detection, preparation of entangled states, cooling of mechanical mode to its ground state of motion. Some associated remarkable phenomena are optomechanically induced transparency and slow light. Here, we investigate these features in the context of parity-time ($\mathcal{PT}$) symmetry. For that purpose, we analyze a system composed of a cavity coupled to pair of $\mathcal{PT}$ symmetric mechanical resonators, and investigate the first-order sidebands induced by the radiation pressure on the cavity end-mirror. System is driven by a strong control field and a weak probe field. Using a perturbative method in resolved sideband regime, we observe the transmission of the probe field and slow light around the exceptional point. System exhibits different behaviors in $\mathcal{PT}$ broken and $\mathcal{PT}$ unbroken phases. In addition to these, we apply polaron transformation, and compare our results with the previous approach. Finally, we offer a preliminary exposition of phase relations for a ternary coupled $\mathcal{PT}$ symmetric system, where both mechanical resonators are coupled to the electromagnetic cavity which exemplifies higher-order exceptional points. Predominantly, our results highlight the effects of $\mathcal{PT}$ symmetry and exceptional points on the optomechanically induced transparency.

Keywords: $\mathcal{PT}$ symmetry, exceptional points, optomechanically induced transparency, polaron transformation, slow light.

ÖZET

$\mathcal{PT}$ SİMETRİK BİR SİSTEMDE OPTOMEKANİKSEL İRGİTİMLİ SAYDAMLIK

Beyza Sütlüoğlu
Fizik, Yüksek Lisans
Tez Danışmanı: Ceyhun Bulutay
Ağustos 2020

Optomekanik sistemler yakın zamanda fiziğin birçok alanında dikkat çekmiştir ve lazer soğutma, kütleçekim dalgalarının tespiti, dolaşık durumların elde edilmesi, mekanik kipin taban durum hareketine soğutulması gibi amaçlarla kullanılmıştır. Bununla birlikte optomekaniksel irgitimli saydamlık, yavaş ışık gibi özellikler de gözlemlenebilmektedir. Bu çalışmada parite-zaman ($\mathcal{PT}$) simetrisi bağlamında bu özellikleri incelemekteyiz. Bu amaç doğrultusunda $\mathcal{PT}$ simetrik iki mekanik çınlacın pasif olanı ile çiftlenmiş bir kovuktan oluşan sistemi analiz etmekteyiz. Öncelikli hedefimizi kovuğun çınlaca bağlı olan aynasının hareketinden kaynaklanan birinci derece yanbantları incelemek oluşturmaktadır. Sistem güçlü bir kontrol ve zayıf bir sonda lazeri ile sürülmektedir. Yanbant çözünür rejiminde pertürbatif metot kullanarak sonda alanının iletimini ve yavaş ışık özelliğini istinai nokta civarında mercek altına almaktayız. Yukarıda bahsettiğimiz yönteme ek olarak sisteme polaron dönüşümü uygulayıp iki yaklaşımı karşılaştırmaktayız. En nihayetinde yüksek dereceli istisnai nokta özelliği göstermesini beklediğimiz üçlü olarak çiftlenmiş bir optomekanik sistem için bir ön çalışma mahiyetinde faz ilişkilerini incelemekteyiz.

Anahtar sözcükler: $\mathcal{PT}$ simetri, istisnai nokta, optomekaniksel irgitimli saydamlık, polaron dönüşümü, yavaş ışık.

Acknowledgement

I gratefully thank my advisor Ceyhun Bulutay for all his guidance and support during my undergraduate and graduate years. I could not imagine a better thesis process.

I would like to thank my thesis committee Oğuz Gülseren and Cem Yüce for their valuable comments and times.

I want to thank sincerely my dearest mother and my dearest sister for their love and support throughout my life.

I would like to thank Mert for his love and understanding, he made my life so beautiful in Bilkent.

Finally, this thesis is dedicated to my beloved father who raised and made me the person who I am.

Contents

List of Figures

Chapter 1

Introduction

1.1 A Brief History of Optomechanics

Cavity optomechanics relies on the mutual interaction between confined electromagnetic field and the mechanical motion mediated by radiation pressure. It has been a rapidly growing field in recent years and many experiments paved the way for both gravitational wave detection, monitoring mechanical motion and preparation of entangled states [1, 2, 3, 4, 5, 6]. As the pioneer of this field, Ashkin demonstrated a method for trapping atoms and cooling gases using resonance radiation pressure of highly focused laser beams and atomic injections [7]. Even earlier, radiation pressure was also used to cool the mechanical motion by laser radiation [8]. Realization of laser cooling experimentally led many applications such as optical atomic clock and measurement of gravitational fields precisely [9]. Idea of turning one end of optical cavity to a harmonic oscillator was proposed by Braginsky *et al* where they demonstrated damping of mechanical motion induced by radiation pressure [10]. In 1983, radiation pressure induced bistability and mirror confinement experiment performed by Dorsel and coworkers gave rise to novel applications for interferometric measuring of mechanical displacements accurately [11].

Discrete nature of photons induces quantum fluctuations in the radiation pressure. Braginsky asserted that radiation pressure of light in a resonator causes quantum back action due to the quantum fluctuations and this effect imposes the standart quantum limit on accuracy of position of free mass measurement [12, 13]. Additionally, standart quantum limit for the position detection evoked a great amount of attention for sensitive measurement of mechanical motion and gravitational wave detectors such as LIGO [14, 15, 16, 17]. Sensitivity of the interferometers is actually disturbed by both dynamic and quantum back-action. Their use for atomic laser cooling of mechanical motion was reviewed in Kippenberg and Vahala's article demonstrating the differences between dynamic and quantum back-action [18]. Moreover, it was shown that generation of nonclassical states like Schrödinger cat state can be produced by utilizing an optomechanical system consisting of a resonator with movable mirror due to the arising entanglement between optical cavity mode and the mechanical mode [19, 20, 21, 22].

Eliminating the thermal effects in optomechanical systems makes easier to observe quantum effects and this can be achieved by cooling of mechanical modes to ground state of motion. In 2000's, the research in optomechanical cooling has experienced an impetus [23, 24, 25], to directions such as resolved sideband limit and the strong coupling regime [26, 27]. Further interesting phenomena scrutinized in this era were optomechanically induced transparency (OMIT), slow light, anti bunching in photon correlations [28, 29, 30, 31].

1.2 Optomechanically Induced Transparency

Especially OMIT attracted remarkable attention since 2010 [32]. It was conceived theoretically as an analog of electromagnetically induced transparency [33], and was rapidly demonstrated experimentally [34, 29]. Afterwards, tunable multichannel cases which are double and multiple OMIT were also explored [35, 36, 37]. It has been shown that transparency window could be observed for different kind of optomechanical systems such as quadratically coupled [38], assisted by a two

level atomic ensemble which enables a controllable OMIT [39], mechanical resonator driven by a coherent field which can adjust the transmission of light from absorption to amplification [40], and also for a coupled double cavity configuration producing an electromagnetically induced absorption within a transparency window [41]. Optomechanically induced transparency paved an avenue for novel applications such as manipulation of light propagation where the group velocity of light can be decreased remarkably like in the case of electromagnetically induced transparency [33], for making precision measurements of weak magnetic fields [42], electric charges [43] and environmental temperature [44].

1.3 $\mathcal{PT}$ Symmetry

The other pillar of this thesis is the $\mathcal{PT}$ symmetric quantum mechanics where real spectra can be observed in non-Hermitian Hamiltonians which are invariant under $\mathcal{PT}$ transformation contrary to conventional idea of only Hermitian Hamiltonians having real eigenvalues. It goes backs to at least 1998, when Bender and his coworkers realized the importance of $\mathcal{PT}$ symmetry as well as the phase transition which occurs at the so-called exceptional point. Later on a generalization to complex quantum mechanics was made by introducing a C operator [45, 46, 47]. However, a complete mathematical proof of reality of the spectra for $\mathcal{PT}$ symmetric quantum mechanical systems was made by Dorey and his colleagues [48, 49]. In 2002, Mostafazadeh introduced the concept of pseudo-Hermiticity, and asserted that all Hamiltonians having real eigenvalue spectrum are pseudo-Hermitian, and the $\mathcal{PT}$ symmetric Hamiltonians are actually a subset of these Hamiltonians [50]. In his subsequent works, necessary and sufficient conditions were given to have a real eigenvalue spectrum in non-Hermitian Hamiltonians, and proved that pseudo-Hermiticity is the necessary condition accompanied with a linear invertible operator [51, 52]. Nevertheless, the community largely concentrated on the $\mathcal{PT}$ symmetric systems rather than the broader class of pseudo-Hermitian ones.

1.4 Examples of $\mathcal{PT}$ Symmetric Systems

The main thrust behind the $\mathcal{PT}$ symmetric systems is the experimental evidence behind it. After the initial theoretical interest around the turn of this century, the momentum behind it was in the decline until 2010, when the field literally exploded with the experimental demonstration of $\mathcal{PT}$ symmetry in optics [53]. Thus, not surprisingly $\mathcal{PT}$ symmetric systems have attracted a considerable amount of attention in the framework of photonics [54, 55, 56]. To test the $\mathcal{PT}$ symmetric systems experimentally, optical systems having complex refractive indexes were used instead of the complex potentials in non-Hermitian Hamiltonians [57, 58, 59]. Furthermore, it has been shown that $\mathcal{PT}$ symmetric optical systems enabled many important applications such as double refraction and power oscillations due to eigenvector unfolding in exact phase, non-reciprocal light transmission and observation of edge states in topological insulators [57, 60, 61, 62]. Additionally, loss induced transparency, a system acting as both laser and coherent perfect absorber at the same time and, effects of spontaneous breaking of $\mathcal{PT}$ symmetry on microring lasers were demonstrated [63, 64, 65, 66, 67, 68]. $\mathcal{PT}$ symmetric optomechanical system with the controlled loss and gain offers a remarkable resource due to its unique characteristics around exceptional points like ultralow-threshold phonon laser, chaos, OMIT and slow light [69, 70, 71, 72]. These features stemming from exceptional point are the motivation for us to study optomechanically induced transparency and slow light in $\mathcal{PT}$ symmetric optomechanical system.

1.5 This Thesis

In this work, we consider a system including a cavity and a pair of $\mathcal{PT}$ symmetric mechanical resonators to reveal how OMIT and slow light come about by the noteworthy features of $\mathcal{PT}$ symmetry and exceptional points.

Chapter 2 introduces $\mathcal{PT}$ symmetry, and makes a brief geometric explanation

of exceptional points which form the essence of this thesis since the system undergoes a phase transition, and eigenvalues simultaneously coalesce with eigenvectors at this point [45, 47]. In Chapter 3, for a three-mode Λ type system composed of a cavity coupled to passive one of $\mathcal{PT}$ symmetric mechanical resonators, we show OMIT and slow light in both $\mathcal{PT}$ broken and $\mathcal{PT}$ unbroken phases using a perturbative method which restricts to the first-order sidebands while system is driven coherently by a strong control field and a weak probe field. For the remainder of Chapter 3, we implement the polaron transformation method, and diagonalize the modified Hamiltonian in absence of the external driving fields. We compare the two approaches when system transits from $\mathcal{PT}$ symmetric phase to $\mathcal{PT}$ broken phase.

In Chapter 4, we extend the optomechanical system so that cavity and two mechanical resonators are all inter-coupled. We investigate the effects of additional coupling on the OMIT as the phase of one of the coupling coefficients is varied. In the Conclusion chapter, we review our results and suggest a route for future work based on our results.

Chapter 2

Parity Time Symmetry and Exceptional Points

2.1 Parity Time Symmetry

In most textbook examples of quantum mechanics, systems are isolated and closed, meaning that they do not exchange energy and particles with the environment. In the Hamiltonian formulation, such systems are described by a Hermitian matrix which is invariant under matrix transposition and complex conjugation. Hermitian Hamiltonians have always real eigenvalues, total energy and probability are conserved, since probability is constant in time; as a direct implication the time evolution operator becomes unitary. As for the more realistic open physical systems coupled to an environment, the systems energy is not fixed, and it can have gain or loss [73]. Such systems are described by non-Hermitian Hamiltonians if we consider only the system subspace [74]. Historical examples of open systems are alpha decay described by Gamow as the escape of an electron from the nuclei, and the complex potential which was used to describe by Feshbach, Porter and Weisskopf for the scattering between nuclei and neutrons. Difference of such Hamiltonians from the Hermitian ones is that they have complex eigenvalues and

due to complexity of energy, alpha decay via tunneling and scattering interactions can be explained. However, non-Hermitian Hamiltonians having parity and time symmetry have real eigenvalues [56]. Those $\mathcal{PT}$ symmetric systems lie between open and closed systems. The reason for that is the system is in contact with environment but also it is in equilibrium. Example of such a system is two coupled boxes which experience equal amount of gain and loss (see Figure 2.1). Corresponding $\mathcal{PT}$ symmetric Hamiltonian for such a system is

$$\hat{H}_{combined} = \begin{bmatrix} a+ib & g \\ g & a-ib \end{bmatrix}, \tag{2.1}$$

where g is a real coupling constant and imaginary part b on the diagonals determines whether system has gain or loss. Under time reversal symmetry gain becomes loss and loss becomes gain. Under space reflection (parity) boxes are swapped [73]. In mathematical terms, time reversal $\hat{T}$ corresponds to a complex conjugation operator, and parity for a bipartite system is represented by the swapping matrix multiplication $\hat{P}=\begin{bmatrix} 0 & 1 \\ 1 & 0 \end{bmatrix}$ [75, 73].

2.2 Exceptional Points

Non-Hermitian degeneracies, also called exceptional points (EP) are singularities in the eigenvalue spectra resulting in coalescence of eigenvectors so that the system reduces its dimensionality by the degree of the EP [74]. EP's are functions of parameters of complex part of the Hamiltonian. In other words, for $\mathcal{PT}$ symmetric systems, phase transition occurs at EP meaning that at one side of EP, eigenvalues are real while at the other side eigenvalues become complex pairs. For the matrix in Eq. (2.1), eigenvalues are $E_{1,2} = a \pm \sqrt{g^2 - b^2}$. When $g < b$ eigenvalues are complex, system is not in equilibrium and in the $\mathcal{PT}$ broken phase, when $g > b$ eigenvalues become real and system is in equilibrium and in the $\mathcal{PT}$ unbroken phase. At $g = \pm b$, phase transition occurs, both eigenvalues and eigenvectors

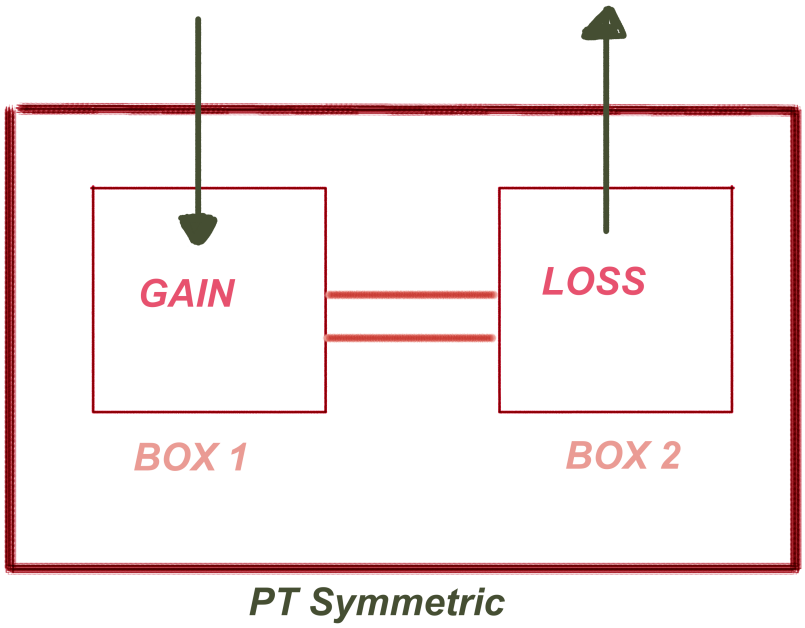

Figure 2.1: Schematic representation of a $\mathcal{PT}$ symmetric system. Two coupled boxes which are in contact with environment experience the same amount of loss and gain.

coalesce [73].

As for the geometric explanation of EP, first Riemann surfaces must be defined. Multi-valued functions like square root function are defined on a Riemann surface. To encircle a point on a Riemann surface, one must rotate twice to return starting point. This is the reason that non-Hermitian Hamiltonians' eigenvalues (energy levels) are defined with two-sheet Riemann surface for a two state problem. A two-state Hamiltonian is represented by $\begin{bmatrix} a & g \\ g & b \end{bmatrix}$, with the energy eigenvalues, $E_{\pm} = \frac{a+b}{2} \pm \frac{1}{2}\sqrt{(a-b)^2 + 4g^2}$. Singularities for the eigenvalues are on the imaginary axis and energy is defined on two-sheet Riemann surface. On complex g surface, quantum levels are not discrete, $g = \pm\frac{|a-b|}{2}i$.
That is why, eigenvalues of non-Hermitian Hamiltonians are described by Riemann surfaces. Non-Hermitian degeneracies (EP) are branch points of the corresponding Riemann sheets and encircling the degeneracy results in replacing of eigenvalues and eigenvectors [74]. This is related to the geometry of the Riemann

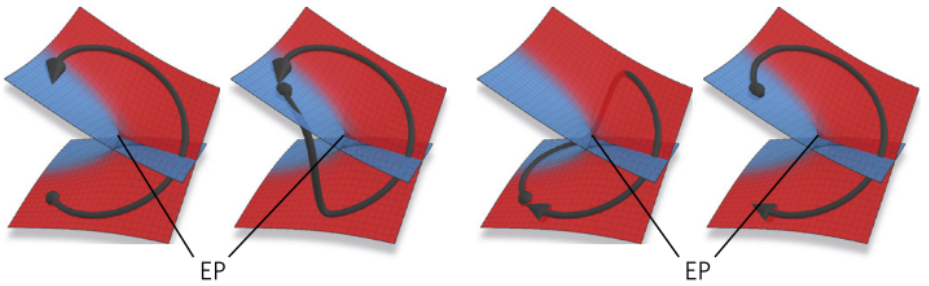

Figure 2.2: Representation of Riemann sheet and encircling an EP, adapted from Ref. [56]

surfaces describing the eigenvalues (see Figure 2.2). Replacing the eigenvalues means that encirclement of exceptional point, beginning at one sheet ends at another one apart from the Berry phase, a second encirclement is necessary to reach the beginning point. Another sheet means that interchanging of the eigenvalues and eigenvectors [56].

2.3 Tools for Non-Hermitian Systems

For non-Hermitian systems, conventional quantum mechanics can not be used but different methods, namely dilation, defining a metric G, and also using an operator C were introduced in literature. [76, 77, 75]. $\mathcal{PT}$-symmetric Hamiltonian can be dilated to a higher dimensional Hermitian Hamiltonian by using an ancilla. However, this method can only be used for unbroken $\mathcal{PT}$ symmetric Hamiltonians; for systems which undergo a phase transition dilation method cannot be used in broken phase [76]. Another method is to define a Hermitian metric operator $G(t)$ that relates non-Hermitian dual state vector to dual Hermitian state vector and with this metric operator equation of motion, inner product, complex conjugation and completeness relations are defined in non-Hermitian quantum mechanics which does not look so different than the conventional one visually [77]. Lastly, a linear operator C commuting with unbroken $\mathcal{PT}$ symmetric Hamiltonian is used to define inner product and an unitary evolution for states [75, 78].

Chapter 3

Optomechanically Induced Transparency in $\mathcal{PT}$ Symmetric System

Optomechanically induced transparency (OMIT) is a quantum interference effect arising due to the different phonon excitation pathways, and within the OMIT window it eliminates the response of the medium like absorption, self focusing and defocusing [34, 79]. System basically consists of a Fabry-Pérot type resonator with a movable end, like a mass attached to a spring. A strong control laser is used to drive the system and a weak probe laser is used to measure the response of this driven optomechanical system. When probe detuning matches with the mechanical resonance frequency, transparency window is observed in the probe transmission spectra [34]. As another aim of this chapter, following Refs. [72, 27], we would like to study the effect of $\mathcal{PT}$ symmetry and EP.

This chapter discusses two approaches to observe OMIT for a $\mathcal{PT}$ symmetric optomechanical system. First one is the formulation in Ref. [27], and the second one utilizes the polaron transformation. Both of them are generally consistent with each other, but since the resulting Hamiltonians are not identical, we also

demonstrate some differences as discussed below. Deliberately we include a detailed account of the formulation so as to fix some critical omissions and typos in the pioneering Ref. [27].

3.1 The Hamiltonian

We consider a three-mode Λ type system which consists of a Fabry-Pérot cavity attached to a pair of coupled $\mathcal{PT}$ symmetric mechanical resonators. The active one is with gain while the passive one experiences equal amount of loss (see Figure 3.1).

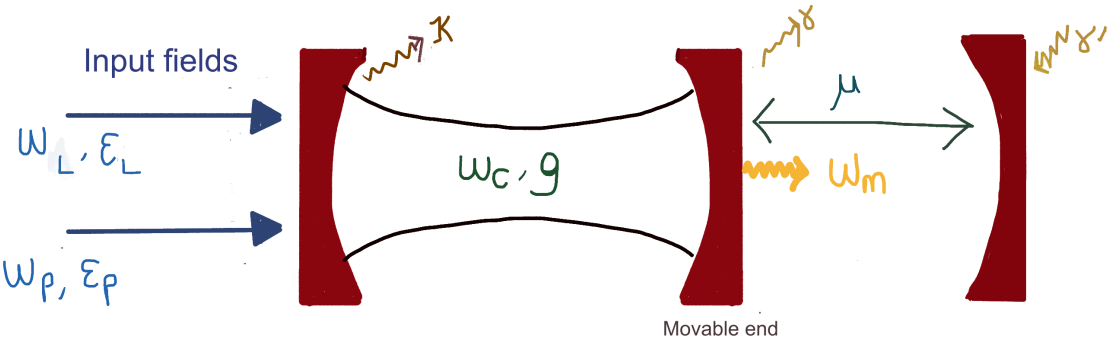

Figure 3.1: Schematic diagram of the $\mathcal{PT}$ symmetric optomechanical system consisting of a cavity with movable end having frequency ω_m. Active mechanical resonator is coupled to passive one with coupling constant, μ.

Cavity with resonance (angular) frequency ω_c is driven with a strong control field with frequency w_l and amplitude ϵ_l, and is probed with a probe field with ω_p and ϵ_p; amplitudes are related to power of the field via equation $\varepsilon_i = \sqrt{\frac{P_i}{\hbar\omega_i}}$,

where index i stands for l, p [1]. For such a system the overall Hamiltonian is

$$\begin{aligned}
\hat{H}_{cavity} &= \hbar\omega_c \hat{a}^\dagger \hat{a}, \\
\hat{H}_{mechanical} &= \hbar\omega_m(\hat{b}_1^\dagger \hat{b}_1 + \hat{b}_2^\dagger \hat{b}_2) - \hbar\mu(\hat{b}_1^\dagger \hat{b}_2 + \hat{b}_2^\dagger \hat{b}_1), \\
\hat{H}_{interaction} &= \hbar g \hat{a}^\dagger \hat{a}(\hat{b}_1^\dagger + \hat{b}_1), \\
\hat{H}_{drive} &= i\sqrt{\eta\kappa}\varepsilon_{l,p}(e^{-i\omega_{l,p}t}\hat{a}^\dagger - e^{i\omega_{l,p}t}\hat{a}),
\end{aligned} \tag{3.1}$$

where $\hat{a}, \hat{b}_1, \hat{b}_2$ are cavity and mechanical mode operators respectively, g is the coupling constant between cavity mode and the passive mechanical mode arising from radiation pressure inside the cavity, κ is the cavity decay rate, and η is the coupling parameter.

3.2 Rotating Frame Transformation

Optomechanical system depends on time due to driving as it is seen from the Hamiltonian in Eq. (3.1). Unitary transformation is applied to remove the time dependency in the driving Hamiltonian in a way that the system is observed in a rotating frame with frequency ω_l. Note that we do not introduce any approximation with this transformation. Hamiltonian takes the following form with the unitary operator

$$\begin{aligned}
\hat{U}(t) &= e^{-i\hbar\omega_l \hat{a}^\dagger \hat{a} t}, \\
\hat{H} &= \hat{U}^\dagger \hat{H}(t) \hat{U} - i\hat{U}^\dagger \frac{\partial \hat{U}}{\partial t}.
\end{aligned} \tag{3.2}$$

Second term in the transformed Hamiltonian is called as the gauge term and detunings for probe and control lasers arise due to the this term where Hamiltonian is obtained using Baker–Campbell–Hausdorff formula

$$e^{\hat{A}} \hat{B} e^{-\hat{A}} = \hat{B} + \left[\hat{A}, \hat{B}\right] + \frac{1}{2!}\left[\hat{A}, \left[\hat{A}, \hat{B}\right]\right] + ..., \tag{3.3}$$

$$\begin{aligned}
\hat{H} =& \hbar\Delta \hat{a}^\dagger \hat{a} + \hbar\omega_m(\hat{b}_1^\dagger \hat{b}_1 + \hat{b}_2^\dagger \hat{b}_2) - \hbar\mu(\hat{b}_1^\dagger \hat{b}_2 + \hat{b}_2^\dagger \hat{b}_1) - \hbar g \hat{a}^\dagger \hat{a}(\hat{b}_1^\dagger + \hat{b}_1) \\
&+ i\hbar\sqrt{\eta\kappa}\varepsilon_l(\hat{a}^\dagger - \hat{a}) + i\hbar\sqrt{\eta\kappa}\varepsilon_p(\hat{a}^\dagger e^{-i\omega t} - \hat{a}e^{i\omega t}),
\end{aligned} \tag{3.4}$$

[1] In Ref. [27], there is confusion of indexes for both cavity and control lasers, same index (c) is used for referring both of them where in some places also index l is used for control field frequency.

where we define $\Delta \equiv \omega_c - \omega_l$, $\omega \equiv \omega_p - \omega_l$, and μ is the coupling constant between mechanical resonators. Therefore, the so-called detuning frequency ω in the system is controlled by changing the probe field frequency while the frequency of control laser is fixed.

3.3 Heisenberg-Langevin Equations

Next step is to obtain the Heisenberg-Langevin (HL) equations to determine the time evolution of cavity and mechanical modes in the presence of gain and loss. Dissipation is introduced with Markov approximation, and the essential evolution comes exactly from the Heisenberg equation of motion (EOM) of an operator

$$\dot{\hat{a}} = \frac{-i}{\hbar}\big[\hat{a}, \hat{H}\big]. \tag{3.5}$$

Thus, EOM's for the mode operators are

$$\begin{aligned}
\frac{d\hat{a}}{dt} &= -i\Delta\hat{a} + ig\hat{a}(\hat{b}_1^\dagger + \hat{b}_1) + \sqrt{\eta\kappa}\epsilon_l + \sqrt{\eta\kappa}\varepsilon_p e^{-i\omega t} - \frac{\kappa}{2}\hat{a}, \\
\frac{d\hat{b}_1}{dt} &= -i\omega_m\hat{b}_1 + i\mu\hat{b}_2 + ig\hat{a}^\dagger\hat{a} - \frac{\gamma}{2}\hat{b}_1, \\
\frac{d\hat{b}_2}{dt} &= -i\omega_m\hat{b}_2 + i\mu\hat{b}_1 + \frac{\gamma'}{2}\hat{b}_2,
\end{aligned} \tag{3.6}$$

where γ, γ' are corresponding loss and gain of mechanical resonators. Position of the first mechanical oscillator is defined as $\hat{x} = x_{ZPF}(\hat{b}_1^\dagger + \hat{b}_1)$, where $x_{ZPF} = \sqrt{\frac{\hbar}{2m\omega_m}}$ is the zero point fluctuation of the mechanical oscillator [1].

In the semiclassical approximation, operators become equal to their expectation values since quantum fluctuations are ignored. Steady state solutions of these HL equations are found by setting time derivative to zero and three coupled equations are obtained for steady state solutions of photon and phonon mode operators. First, $\bar{b}_2$ is obtained from $\frac{db_2}{dt} = 0$ and then using this, $\bar{b}_1$ and successively

$\bar{a}$ is obtained by ignoring the time dependent part in the probe field as [2]

$$\begin{aligned}
\bar{a} &= \frac{\sqrt{\eta\kappa}\varepsilon_l}{i\Delta + \frac{\kappa}{2} - ig(\bar{b}_1^* + \bar{b}_1)}, \\
\bar{b}_1 &= \frac{ig(i\omega_m - \gamma'/2)|\bar{a}|^2}{(i\omega_m + \gamma/2)(i\omega_m - \gamma'/2) + \mu^2}, \\
\bar{b}_2 &= \frac{i\mu\bar{b}_1}{i\omega_m - \gamma'/2}.
\end{aligned} \tag{3.7}$$

3.4 Linearization

To linearize the system, the ansatz $\hat{\aleph} = \bar{\aleph} + \delta\aleph$ is used within semiclassical approximation $\hat{a} \equiv \langle\hat{a}\rangle, \hat{b}_{1,2} \equiv \langle\hat{b}_{1,2}\rangle$. Substituting this ansatz to HL equations and ignoring the nonlinear terms, EOM's of perturbation terms are found, and linearization discards higher-order sidebands that are actually generated in coupled optomechanical systems [80]. Substituting the ansatz to first equation of Eq. (3.6) yields

$$\frac{d\delta a}{dt} = -i\Delta(\bar{a} + \delta a) + ig(\bar{a} + \delta a)(\bar{b}_1^* + \delta b_1^* + \bar{b}_1 + \delta b_1) + \sqrt{\eta\kappa}\varepsilon_l + \sqrt{\eta\kappa}\varepsilon_p e^{-i\omega t} - \frac{\kappa}{2}(\bar{a} + \delta a). \tag{3.8}$$

Using the first equation of Eq. (3.7), evolution of the perturbation term for intracavity mode is found as

$$\frac{d\delta a}{dt} = -i\Delta\delta a - \frac{\kappa}{2}\delta a + ig\delta a(\bar{b}_1^* + \bar{b}_1) + ig\bar{a}(\delta b_1^* + \delta b_1) + \sqrt{\eta\kappa}\varepsilon_p e^{-i\omega t}. \tag{3.9}$$

Substituting the ansatz $\hat{b}_{1,2} = \bar{b}_{1,2} + \delta b_{1,2}$ and then inserting the steady state equations to appropriate places, EOM for the perturbation terms are found after some algebra as

$$\begin{aligned}
\frac{d\delta b_1}{dt} &= -i\omega_m\delta b_1 - \frac{\gamma}{2}\delta b_1 + ig(\bar{a}\delta a^* + \bar{a}^*\delta a) + i\mu\delta b_2, \\
\frac{d\delta b_2}{dt} &= -i\omega_m\delta b_2 + \frac{\gamma'}{2}\delta b_2 + i\mu\delta b_1.
\end{aligned} \tag{3.10}$$

[2] Steady state value of intracavity mode Eq. (3) in Ref. [27] has a typo. Sign before the coupling constant in the denominator must be minus.

3.5 Transmission of the Probe

These coupled differential equations can be solved via inserting a perturbative solution. The idea behind this is to find the amplitude of the anti-Stokes field (see Figure 3.2) for a given $\omega = \omega_p - \omega_l$. Driven optomechanical system annihilates and creates photon at the first-order sidebands and transmission probability of the probe is found from anti-Stokes field's amplitude [32]. If one wants to demonstrate the effects of the nonlinearity in the system, higher order sidebands must be retained. However, for our case, first-order sideband which amounts to the linear case is sufficient to see the transparency window [27]. As it will be seen in the following plots, transparency window appears when $\omega \approx \omega_m$, and the reason behind this is time dependent radiation pressure providing a modulation frequency ω. When this frequency becomes resonant with the frequency of mechanical resonator, they start to oscillate coherently, and create the first order sidebands. Anti-Stokes field becomes resonant with probe frequency inside the cavity mode. Then, destructive interference between these two fields suppresses the intracavity field, and since probe field measures the photon mode transitions inside cavity, there appears a transparency window [32].

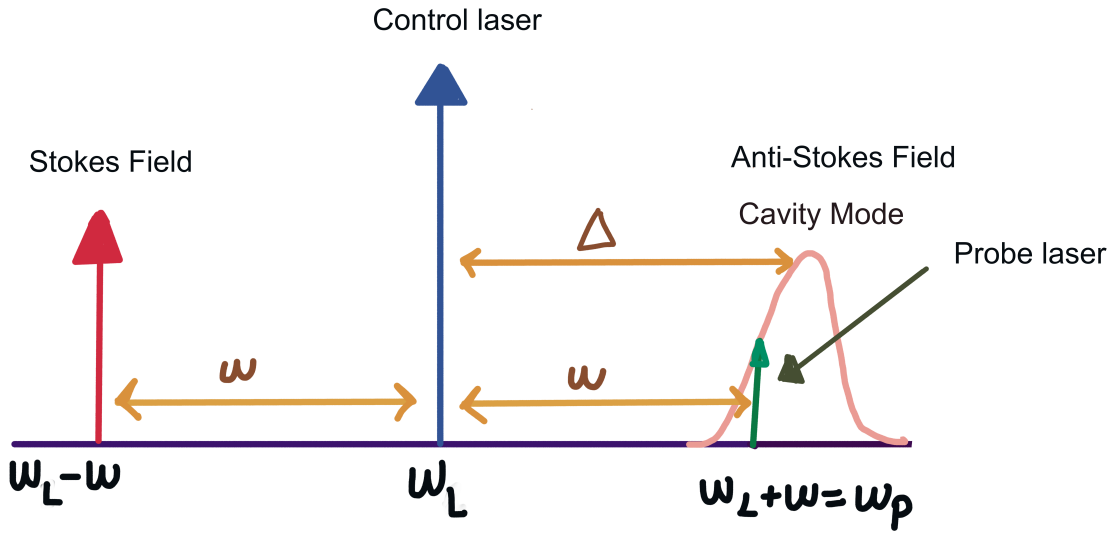

Figure 3.2: The frequency configuration of Stokes and anti-Stokes fields

$$
\begin{aligned}
\delta a &= A_{1+}e^{i\omega t} + A_{1-}e^{-i\omega t},\\
\delta b_1 &= B_{1+}e^{i\omega t} + B_{1-}e^{-i\omega t},\\
\delta b_2 &= C_{1+}e^{i\omega t} + C_{1-}e^{-i\omega t}.
\end{aligned}
\tag{3.11}
$$

After substituting these equations into coupled differential equations and separating equations with the same complex exponentials, amplitudes of the first-order sidebands are found. Substitution yields

$$
\begin{aligned}
A_{1+}i\omega &= A_{1+}\Big(-i\Delta - \frac{\kappa}{2} + ig(\bar{b}_1 + \bar{b}_1^*)\Big) + ig\bar{a}(B_{1+} + B_{1-}^*),\\
-A_{1-}i\omega &= A_{1-}\Big(-i\Delta - \frac{\kappa}{2} + ig(\bar{b}_1 + \bar{b}_1^*)\Big) + ig\bar{a}(B_{1-} + B_{1+}^*) + \sqrt{\eta\kappa}\varepsilon_p,\\
B_{1+}i\omega &= B_{1+}(-i\omega_m - \frac{\gamma}{2}) + (ig\bar{a}A_{1-}^* + ig\bar{a}^*A_{1+}) + C_{1+}i\mu,\\
-B_{1-}i\omega &= B_{1-}(-i\omega_m - \frac{\gamma}{2}) + (ig\bar{a}A_{1+}^* + ig\bar{a}^*A_{1-}) + C_{1-}i\mu,\\
C_{1+} &= \frac{i\mu}{i\omega + i\omega_m - \gamma'/2}B_{1+},\\
C_{1-} &= \frac{i\mu}{-i\omega + i\omega_m - \gamma'/2}B_{1-}.
\end{aligned}
\tag{3.12}
$$

Next, equations for $C_{1\pm}$'s are substituted into equations for $B_{1\pm}$'s to decouple them step by step

$$
\begin{aligned}
B_{1+} &= \frac{ig(\bar{a}A_{1-}^* + \bar{a}^*A_{1+})}{i\omega + i\omega_m + \frac{\gamma}{2} + \frac{\mu^2}{i\omega + i\omega_m - \frac{\gamma'}{2}}},\\
B_{1-} &= \frac{ig(\bar{a}A_{1+}^* + \bar{a}^*A_{1-})}{-i\omega + i\omega_m + \frac{\gamma}{2} + \frac{\mu^2}{-i\omega + i\omega_m - \frac{\gamma'}{2}}}.
\end{aligned}
\tag{3.13}
$$

These B_1's are used to decouple the A_1's and finally only A_1's are coupled to each other as

$$A_{1-}\Xi(\omega) = ig\bar{a}\left[\frac{-ig(\bar{a}A_{1-}+\bar{a}A_{1+}^{*})}{-i\omega-i\omega_m+\frac{\gamma}{2}+\frac{\mu^2}{-i\omega-i\omega_m-\frac{\gamma'}{2}}}\right]+ig\bar{a}\left[\frac{ig(\bar{a}^{*}A_{1-}+\bar{a}A_{1+}^{*})}{-i\omega+i\omega_m+\frac{\gamma}{2}+\frac{\mu^2}{-i\omega+i\omega_m-\frac{\gamma'}{2}}}\right] + \sqrt{\eta\kappa}\varepsilon_p, \tag{3.14}$$

where $\Xi(\omega) = i\Delta+\kappa/2-i\omega-ig(\bar{b}_1^{*}+\bar{b}_1)$. As it is seen from this equation to find the the amplitude A_{1-}, A_{1+}^{*} is required, conjugate of the first equation in Eq. (3.12) depends on the B_{1+}^{*} and B_{1-}, substituting these into A_{1+}^{*} following equation is obtained

$$\begin{aligned} A_{1+}^{*}(\Xi(-\omega))^{*} = &-ig\bar{a}^{*}\left[\frac{-ig(\bar{a}^{*}A_{1-}+\bar{a}A_{1+}^{*})\alpha(\omega_m,-\gamma')}{f_1(\alpha)}\right] \\ &-ig\bar{a}^{*}\left[\frac{-ig(\bar{a}A_{1+}^{*}+\bar{a}^{*}A_{1-})\alpha(-\omega_m,-\gamma')}{f_2(\alpha)}\right], \end{aligned} \tag{3.15}$$

with defined set of equations

$$\begin{aligned} \alpha(\omega_m,\gamma) &= -i\omega_m - i\omega + \frac{\gamma}{2}, \\ f_1(\alpha) &= \alpha(\omega_m,\gamma)\alpha(\omega_m,-\gamma') + \mu^2, \\ f_2(\alpha) &= \alpha(-\omega_m,\gamma)\alpha(-\omega_m,-\gamma') + \mu^2. \end{aligned} \tag{3.16}$$

Collecting A_{1+}^{*} in the right hand side, A_{1-} becomes

$$A_{1+}^{*} = \frac{-ig\bar{a}^{*}\lambda}{(\Xi(-\omega))^{*}+ig\bar{a}\lambda}A_{1-}, \tag{3.17}$$

with

$$\lambda = -ig\bar{a}^{*}\left[\frac{\alpha(\omega_m,-\gamma')}{f_1(\alpha)}-\frac{\alpha(-\omega_m,-\gamma')}{f_2(\alpha)}\right]. \tag{3.18}$$

Finally, substituting Eq. (3.17) into Eq. (3.14), amplitude of the first upper sideband having frequency $\omega+\omega_l$ is obtained as[3]

[3]In Ref. [27], Eq. (6) is incorrect. Defined set of equations for $f_2(\alpha)$ and $f_3(\alpha)$ are $f_{1,2}(\alpha)$ here. Equation for $f_1(\alpha)$ in Ref. [27] does not appear in the equations. There are two defined equations in Ref. [27] for λ but only the second one is used whereas first one again does not appear. Furthermore, there is another mistake in frequencies of output fields which is written as $\omega_c \pm \omega$ at the same page, correct frequencies are $\omega_l \pm \omega$.

$$A_{1-} = \frac{\sqrt{\eta\kappa}\varepsilon_p}{\Xi(\omega) - ig\bar{a}(\lambda + \lambda\Gamma^*)}, \tag{3.19}$$

with

$$\Gamma^* = \frac{-ig\bar{a}\lambda}{(\Xi(-\omega))^* + ig\bar{a}\lambda}. \tag{3.20}$$

After finding amplitude, using input-output relationship $S_{out} = S_{in} - \sqrt{\eta\kappa}\langle\hat{a}\rangle$ where $\langle\hat{a}\rangle = \bar{a} + \delta a$, and S_{in} is found from the driving field in rotating frame as $S_{in} = \varepsilon_l + \varepsilon_p e^{-i\omega t}$. Output becomes [4][34, 27]

$$S_{out} = \varepsilon_l - \sqrt{\eta\kappa}\bar{a} + (\varepsilon_p - \sqrt{\eta\kappa}A_{1-})e^{-i\omega t} - \sqrt{\eta\kappa}A_{1+}e^{i\omega t}. \tag{3.21}$$

Here, $\sqrt{\eta\kappa}A_{1+}$ is amplitude of Stokes field and $\epsilon_l - \sqrt{\eta\kappa}\bar{a}$ is the frequency spectra of control field. A_{1+} becomes nearly zero in resolved-sideband regime ($\kappa \ll \omega_m$) [34]. Third term is the amplitude of anti-Stokes field and its division with ϵ_p gives the transmission of probe field from $t_p = (\varepsilon_p - \sqrt{\eta\kappa}A_{1-})/\varepsilon_p$ as

$$t_p = 1 - \frac{\eta\kappa}{\Xi(\omega) - ig\bar{a}(\lambda + \lambda\Gamma^*)}. \tag{3.22}$$

Another effect appearing in such an optomechanical system is the transition from fast to slow light caused by the sign change in group velocity of light at the probe frequency. This can be shown from rapid phase dispersion at ω_p, $\psi(\omega_p) = \arg[t_p(\omega_p)]$. Gradient of dispersion for different probe frequencies leads to the group delay [81, 27]

$$\tau_g = \frac{d\psi(\omega_p)}{d\omega_p}. \tag{3.23}$$

This transition can be adjusted by modulating power of control field and transition point shifts with mechanical coupling constant. Ref. [81] also demonstrates that for an optomechanical $\mathcal{PT}$ symmetric system with two cavity (active, passive) where the passive one is coupled to mechanical resonator driven by a phonon

[4]First term in the output field Eq. (7) in Ref. [27] is ϵ_c which is a typo since this term must be the amplitude of the control field, ϵ_l.

pump, transition from fast ($\tau_g < 0$) to slow ($\tau_g > 0$) light can be tuned with changing the gain and loss ratio, power of control field and phase of phonon pump in the system.

3.6 Non-Hermitian Mechanical Hamiltonian

To find the EP of non-Hermitian mechanical Hamiltonian, its eigenvalues are found as[5]

$$\hat{H}'_M = \begin{pmatrix} \hat{b}_1^\dagger & \hat{b_2}^\dagger \end{pmatrix} \begin{pmatrix} \hbar\omega_m - i\hbar\frac{\gamma}{2} & \mu\hbar \\ \mu\hbar & \hbar\omega_m + i\hbar\frac{\gamma'}{2} \end{pmatrix} \begin{pmatrix} \hat{b}_1 \\ \hat{b}_2 \end{pmatrix}, \tag{3.24}$$

$$\Omega_{1,2} = \hbar\omega_m + \frac{i\hbar(\gamma - \gamma')}{4} \mp \sqrt{\mu^2\hbar^2 - \frac{(\gamma + \gamma')^2}{16}\hbar^2}. \tag{3.25}$$

Loss γ and gain γ' are equal to have a $\mathcal{PT}$ symmetric system with real eigenvalues and EP is the value that makes the radical zero, $\mu = \frac{\gamma+\gamma'}{4}$. Those eigenvalues can also be defined as

$$\begin{aligned} \Omega_{1,2} &= \hbar\omega_\mp + i\hbar\gamma_\mp, \\ \omega_\pm &= \omega_m \pm \mathrm{Re}\left\{\sqrt{\mu^2 - (\frac{\gamma + \gamma'}{4})^2}\right\}, \\ \gamma_\pm &= \frac{\gamma - \gamma'}{4} \pm \mathrm{Im}\left\{\sqrt{\mu^2 - (\frac{\gamma + \gamma'}{4})^2}\right\}, \end{aligned} \tag{3.26}$$

where $\omega_\pm$ are frequencies of dressed states and $\gamma_\pm$ designate the decay of these two mechanical supermodes. The theory will shaped around these parameters. Next section is another formulation of OMIT which uses the polaron transformation.

[5]Hamiltonian matrix Eq. (11) has a trivial typo in Ref. [27], $\hbar$'s are missing.

3.7 Polaron Transformation

As the first step, $\mathcal{PT}$ symmetric coupled mechanical resonators are diagonalized as

$$\hat{H}_M = \Omega_1 \hat{B}_1^\dagger \hat{B}_1 + \Omega_2 \hat{B}_2^\dagger \hat{B}_2, \tag{3.27}$$

where its matrix form is given in Eq. (3.24) and Ω_1 and Ω_2 are the complex eigenvalues of mechanical non-Hermitian Hamiltonian. We can express the phonon mode transformation via

$$\hat{b} = M\hat{B}, \tag{3.28}$$

where for simplicity we introduce $m_1 = M_{11}$ and $m_2 = M_{12}$. These $m_{1,2}$ in transformation matrix are found numerically. Optomechanical Hamiltonian without the driving terms can be diagonalized using polaron transformation. Idea is to introduce the radiation-pressure displaced phonon operators with respect to two mechanical modes with $i = 1, 2$ [82]. [6]

$$\hat{H}_{OM} = \omega_c \hat{n} + \Omega_1 \hat{B_1}^\dagger \hat{B}_1 + \Omega_1 \hat{B_2}^\dagger \hat{B}_2 - g\hat{n}(m_1 \hat{B}_1 + m_2 \hat{B}_2 + h.c). \tag{3.29}$$

To remove the coupling term, i.e nonlinearity, polaron mode operators are introduced as

$$\begin{aligned} \hat{d}_i &\equiv \hat{B}_i - \frac{g m_i}{\Omega_i}\hat{n}, \\ \hat{d_i}^\dagger &\equiv \hat{B}_i^\dagger - \frac{g m_i^*}{\Omega_i^*}\hat{n}. \end{aligned} \tag{3.30}$$

In terms of these new polaron mode operators following optomechanical Hamiltonian is obtained

$$\hat{H}_{OM} = \omega_c \Big[1 - \frac{g^2}{\omega_c \bar{\Omega}}\hat{n}\Big]\hat{n} + \Omega_1 \hat{d_1}^\dagger \hat{d}_1 + \Omega_2 \hat{d_2}^\dagger \hat{d}_2, \tag{3.31}$$

where $\frac{1}{\bar{\Omega}} = \frac{m_1}{\Omega_1} + \frac{m_2}{\Omega_2}$. After diagonalizing the $\hat{H}_{OM}$, external driving fields are coupled to cavity, and then switching to rotating frame with unitary transformation to remove the time dependency in hamiltonian with operator $\hat{U} = e^{i\omega_l t \hat{a}^\dagger a}$. Using

[6] Here, we set $\hbar = 1$ for the remainder of this section.

Baker–Campbell–Hausdorff formula, following $\hat{H}_{OM}$ in rotating frame is obtained as

$$\hat{H}_{OM} = \Delta\Big[1-\frac{g^2}{\Delta\bar{\Omega}}\hat{n}\Big]\hat{n}+\Omega_1\hat{d_1}^\dagger\hat{d}_1+\Omega_2\hat{d_2}^\dagger\hat{d}_2+i\sqrt{\eta\kappa}\varepsilon_l(\hat{a}^\dagger-\hat{a})+i\sqrt{\eta\kappa}\varepsilon_p(\hat{a}^\dagger e^{-i\omega t}-\hat{a}e^{i\omega t}), \tag{3.32}$$

where $\Delta = \omega_c - \omega_l$ and $\omega = \omega_p - \omega_l$. Based on this optomechanical Hamiltonian, following Heisenberg-Langevin equations are found to describe the time dependent motion of cavity and mechanical modes by introducing dissipation term for cavity with Markov approximation where loss and gain of mechanical resonators are introduced previously in mechanical Hamiltonian.

$$\begin{aligned}
\frac{d\hat{a}}{dt} &= -i\Big[\Big(\Delta - i\frac{\kappa}{2}\Big)\hat{a} - \frac{g^2}{\bar{\Omega}}\Big\{\hat{a},\hat{n}\Big\} - g\sum_i \Omega_i\Big(\frac{m_i}{\Omega_i}\hat{d_i}^\dagger\hat{a} + \frac{m_i^*}{\Omega_i^*}\hat{a}\hat{d_i}\Big) + i\sqrt{\eta\kappa}\big(\varepsilon_l + \varepsilon_p e^{-i\omega t}\big)\Big], \\
\frac{d\hat{d_i}}{dt} &= -i\Omega_i\hat{d_i} - \sqrt{\eta\kappa}\frac{gm_i}{\Omega_i}\Big[\big(\varepsilon_l + \varepsilon_p e^{-i\omega t}\big)\hat{a}^\dagger + \big(\varepsilon_l + \varepsilon_p e^{i\omega t}\big)\hat{a}\Big].
\end{aligned} \tag{3.33}$$

Intracavity mode and mechanical mode operators are reduced to their expectation values since quantum fluctuations are ignored, viz. $\hat{a}(t) \equiv \langle\hat{a}(t)\rangle$, $\hat{d}_i(t) \equiv \langle\hat{d}_i(t)\rangle$ within the semiclassical approximation [27]. Before proceeding to the linearization, steady state values for photon and phonon modes must be found by setting $\frac{d\hat{a}}{dt} = 0$ and $\frac{d\hat{d}_i}{dt} = 0$, which yield

$$\begin{aligned}
\bar{a} &= \frac{-i\sqrt{\eta\kappa}\varepsilon_l}{\Delta - i\kappa/2}, \\
\bar{d}_i &= \frac{i\eta\kappa^2 g m_i \varepsilon_l^2}{\Omega_i^2(\Delta^2 + \kappa^2/4)}.
\end{aligned} \tag{3.34}$$

Expressing cavity and mechanical modes as the sum of steady state value and fluctuatiton part i.e $\hat{a} = \bar{a} + \delta\hat{a}$ and $\hat{d}_i = \bar{d}_i + \delta\hat{d}_i$, followed by a linearization procedure for $\delta a \ll \bar{a}$ and evolution of perturbation terms takes the form [34]

$$
\begin{aligned}
\frac{d\delta\hat{a}}{dt} &= -i\Big[(\Delta - i\kappa/2)\delta\hat{a} - \frac{g^2}{\bar{\Omega}} 4\delta\hat{a} \mid \bar{a} \mid^2 - g\delta\hat{a}\sum_i \Omega_i\left(\frac{m_i \bar{d}_i^{\,*}}{\Omega_i} + \frac{m_i^* \bar{d}_i}{\Omega_i^*}\right) \\
&\quad - g\bar{a}\sum_i \Omega_i\left(\frac{m_i \delta\hat{d}_i^*}{\Omega_i} + \frac{m_i^* \delta\hat{d}_i}{\Omega_i^*}\right) + i\sqrt{\eta\kappa}\varepsilon_p e^{-i\omega t}, \\
\frac{d\delta\hat{d}_i}{dt} &= -i\Omega_i \delta\hat{d}_i - \sqrt{\eta\kappa}\frac{g m_i}{\Omega_i}\left[\varepsilon_l \delta\hat{a}^* + \epsilon_l \delta\hat{a} + \varepsilon_p e^{-i\omega t}\bar{a}^* + \varepsilon_p e^{i\omega t}\bar{a}\right].
\end{aligned}
\tag{3.35}
$$

Next step is to solve these set of equations as before with the following sideband terms

$$
\begin{aligned}
\delta\hat{a} &= A_+ e^{i\omega t} + A_- e^{-i\omega t}, \\
\delta\hat{d}_i &= D_{i+} e^{i\omega t} + D_{i-} e^{-i\omega t}.
\end{aligned}
\tag{3.36}
$$

Substituting these to the differential equations and finding the coefficients accompanied by same exponential factor, following set of coupled equations are obtained for $A_\pm$ and $D_{i\pm}$

$$
\begin{aligned}
D_{i+} &= \frac{-\sqrt{\eta\kappa} g m_i\left[\varepsilon_l(A_+ + A_-^*) + \varepsilon_p \bar{a}\right]}{(i\omega + i\Omega_i)\Omega_i}, \\
D_{i-} &= \frac{-\sqrt{\eta\kappa} g m_i\left[\varepsilon_l(A_- + A_+^*) + \varepsilon_p \bar{a}^*\right]}{(-i\omega + i\Omega_i)\Omega_i},
\end{aligned}
$$

$$
\begin{aligned}
A_+\left(-\omega - \Delta + i\frac{\kappa}{2} + \frac{g^2}{\bar{\Omega}} 4|\bar{a}|^2 + g\sum_i \Omega_i 2\,\mathrm{Re}\left\{\frac{m_i \bar{d}_i^*}{\Omega_i}\right\}\right) &= -g\bar{a}\sum_i \Omega_i\left(\frac{m_i}{\Omega_i} D_{i-}^* + \frac{m_i^*}{\Omega_i^*} D_{i+}\right), \\
A_-\left(\omega - \Delta + i\frac{\kappa}{2} + \frac{g^2}{\bar{\Omega}} 4|\bar{a}|^2 + g\sum_i \Omega_i 2\,\mathrm{Re}\left\{\frac{m_i \bar{d}_i^*}{\Omega_i}\right\}\right) &= -g\bar{a}\sum_i \Omega_i\left(\frac{m_i}{\Omega_i} D_{i+}^* + \frac{m_i^*}{\Omega_i^*} D_{i-}\right) \\
&\quad + i\sqrt{\eta\kappa}\varepsilon_p.
\end{aligned}
\tag{3.37}
$$

When $D_{i\pm}$'s are substituted to $A_\pm$, it is seen that to find A_- explicitly, we need A_+^*. Taking first equation in the above set and replacing $D_{i\pm}$ following equation is found

$$
A_+^* = \frac{\Xi\varepsilon_l A_- + \Xi\varepsilon_p \bar{a}^*}{\lambda - \Xi\varepsilon_l},
\tag{3.38}
$$

with

$$\Xi = g^2\bar{a}^* \sum_i \frac{|m_i|^2}{\Omega_i}\sqrt{\eta\kappa}\left(\frac{1}{-i\omega + i\Omega_i} + \frac{1}{-i\omega - i\Omega_i^*}\right),$$
$$\lambda = -\omega - \Delta - \frac{i\kappa}{2} + \frac{g^2}{\bar{\Omega}^*}4|\bar{a}|^2 + g\sum_i \Omega_i^* 2\,\mathrm{Re}\left\{\frac{m_i\bar{d}_i^*}{\Omega_i}\right\}. \tag{3.39}$$

A_+^* depends now only on A_-, substituting $D_{i\pm}$ into the second equation of Eq. (3.37) A_- is obtained

$$A_- = \frac{\varepsilon_l\Gamma}{\Lambda - \Gamma\varepsilon_l}A_+^* + \frac{\Gamma\varepsilon_p\bar{a}^* + i\sqrt{\eta\kappa}\varepsilon_p}{\Lambda - \Gamma\varepsilon_l}, \tag{3.40}$$

with

$$\Lambda = \omega - \Delta + \frac{i\kappa}{2} + \frac{g^2}{\bar{\Omega}}4|\bar{a}|^2 + g\sum_i \Omega_i 2\,\mathrm{Re}\left\{\frac{m_i\bar{d}_i^*}{\Omega_i}\right\},$$
$$\Gamma = g^2\bar{a}\sum_i \frac{|m_i|^2}{\Omega_i^*}\sqrt{\eta\kappa}\left(\frac{1}{-i\omega - i\Omega_i^*} + \frac{1}{-i\omega + i\Omega_i}\right). \tag{3.41}$$

Finally, after replacing the A_+^* and equalizing the denominators, some of the terms will cancel each other and overall amplitude of the first upper sideband will be

$$A_- = \frac{\lambda\Gamma\varepsilon_p\bar{a}^* + i\sqrt{\eta\kappa}\varepsilon_p(\lambda - \Xi\varepsilon_l)}{\lambda\Lambda - \Lambda\Xi\varepsilon_l - \Gamma\lambda\varepsilon_l}. \tag{3.42}$$

Using input-output relation, transmission of probe field becomes

$$t_p = 1 - \sqrt{\eta\kappa}\frac{\lambda\Gamma\bar{a}^* + i\sqrt{\eta\kappa}(\lambda - \Xi\varepsilon_l)}{\lambda\Lambda - \Lambda\Xi\varepsilon_l - \Gamma\lambda\varepsilon_l}. \tag{3.43}$$

3.8 Energy Spectra of $\mathcal{PT}$ Symmetric Optomechanical System

To observe the effects of EP, and the differences between two approaches, first we must explain the relevant states clearly. This is a 3-level Λ type system with energy levels $|\, n, n_{m1}, n_{m2}\rangle$, $|\, n+1, n_{m1}, n_{m2}\rangle$ and $|\, n, n_{m1}+1, n_{m2}\rangle$ where n,$n_{m1,m2}$ are number of photons and phonons, respectively. Weak probe causes a transition

between photonic levels $|\, n, n_{m1}, n_{m2}\rangle$, $|\, n{+}1, n_{m1}, n_{m2}\rangle$ when phonon number stays the same, and the control field leads to phonon transition between $|\, n{+}1, n_{m1}, n_{m2}\rangle$ and $|\, n, n_{m1}+1, n_{m2}\rangle$. There is also a 4th energy level, $|\, n, n_{m1}, n_{m2}+1\rangle$ and transition to this level from $|\, n, n_{m1}+1, n_{m2}\rangle$ is due to the coupling μ between two mechanical resonators. Two dressed states $|\, n, n_{m\pm}\rangle$ are formed because of this coupling between mechanical resonators [see Figure 3.3].

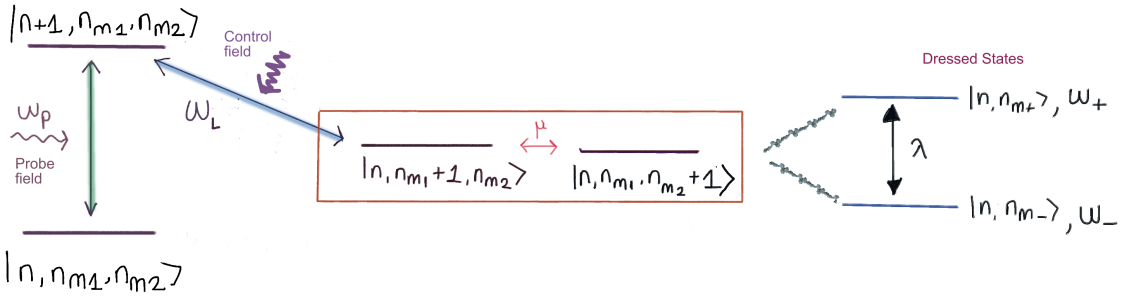

Figure 3.3: Energy level scheme of $\mathcal{PT}$ symmetric optomechanical system.

The frequencies of these two coupled mechanical states are $\omega_\pm$ which we obtained previously when finding the eigenvalues of non-Hermitian mechanical Hamiltonian. Splitting between states are the difference of these frequencies. Depending on coupling constant, energy levels of the system change. First case is, $\mu < \frac{\gamma+\gamma'}{4}$, $\mathcal{PT}$ broken phase. When system is in $\mathcal{PT}$ broken phase, there will not be mode splitting between these states, and frequency becomes $\omega_\pm = \omega_m$ where they have two different decay rates, $\pm\,\mathrm{Im}\left\{\sqrt{\mu^2 - (\frac{\gamma+\gamma'}{4})^2}\right\}$. Obviously, eigenvalues are not real. As for the $\mathcal{PT}$ unbroken phase, $\mu > \frac{\gamma+\gamma'}{4}$, frequency of mechanical supermodes are different but decay rates are degenerate. Splitting width of dressed states is $\lambda = 2\sqrt{\mu^2 - (\frac{\gamma+\gamma'}{4})^2}$ and proportional to coupling constant. At EP, $\mu = \frac{\gamma+\gamma'}{4}$, both eigenvalues and eigenvectors coalesce so that the system dimension is effectively reduced. Dressed state frequencies and dissipation rates become degenerate.

3.9 OMIT Spectra

When probe detuning is equal to mechanical mode frequency, a transparency window is observed, i.e, medium is transparent to this frequency. The physical reason is due to destructive interference between the probe and the anti-Stokes scattered control field so that no build-up of probe within the cavity is possible [34]. At this point, system is in $\mathcal{PT}$ broken phase since there is no mode splitting, only one transparency window is observed. However, when we approach the EP, the peak of the transparency window enhances. For Figure 3.5 around this EP, peak of transparency window increases almost 20 times with respect to previous case which means that this point has a major effect on this physical process, and the reason behind this dependence of transparency window's peak is localization of the strong control field [27]. Moreover, in the unbroken phase since there is a mode splitting, a transition from single OMIT to double OMIT is observed due to the two supermodes.

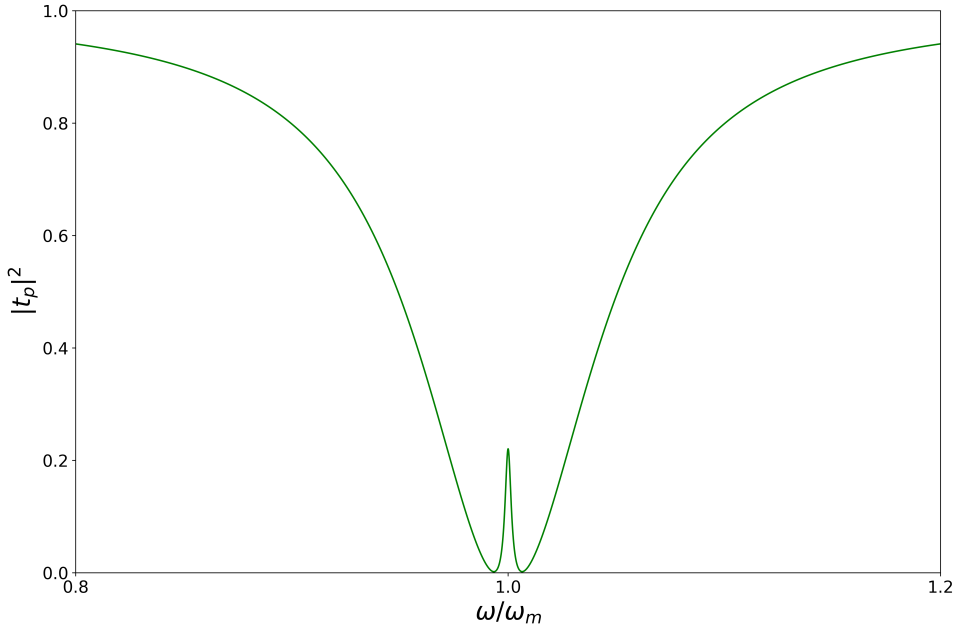

Figure 3.4: Probe power transmission for coefficient mechanical coupling μ = $0.2(\gamma+\gamma')$ with parameters $g = 2\pi$ MHz, $\frac{\omega_m}{2\pi}$ = 3.68 GHz,$\gamma = \gamma' = 0.5\times10^{-2}\omega_m$ and $\kappa = 0.1\omega_m$.

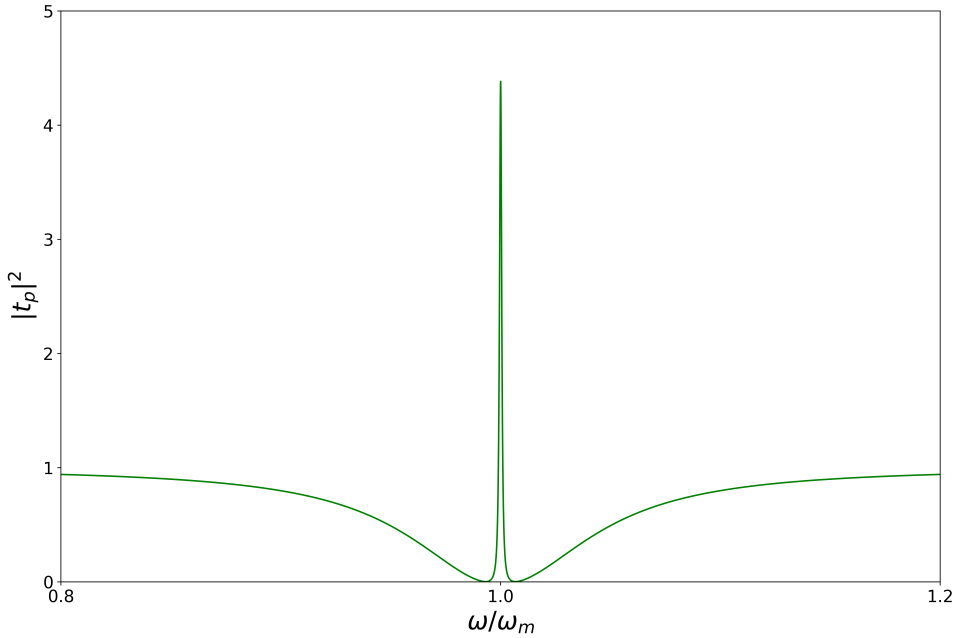

Figure 3.5: Probe power transmission coefficient for mechanical coupling $\mu = 0.27(\gamma + \gamma')$. Other parameters are same as Figure 3.4.

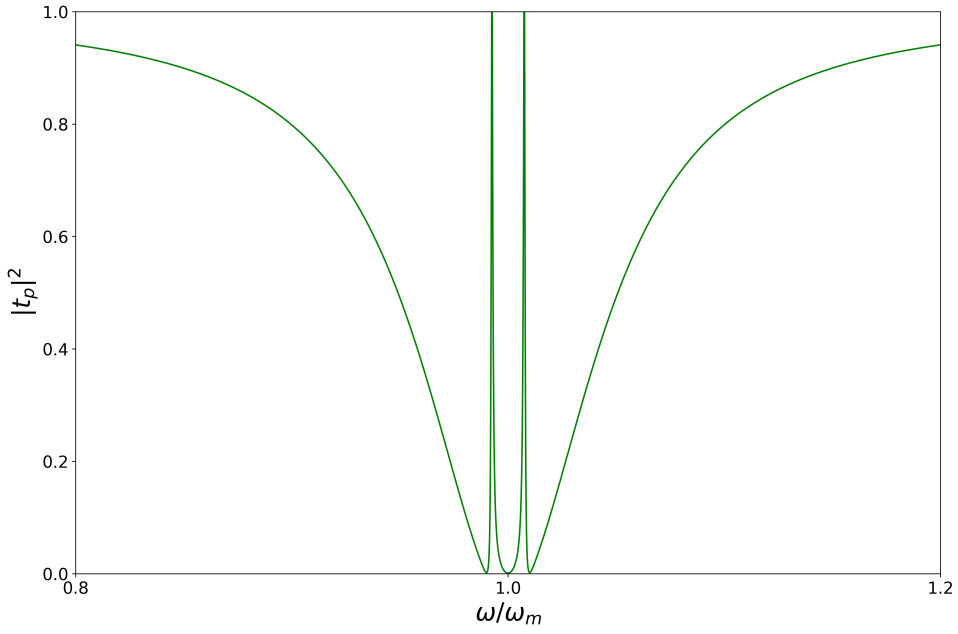

Figure 3.6: Probe power transmission coefficient for mechanical coupling $\mu = 0.8(\gamma + \gamma')$. Other parameters are same as Figure 3.4.

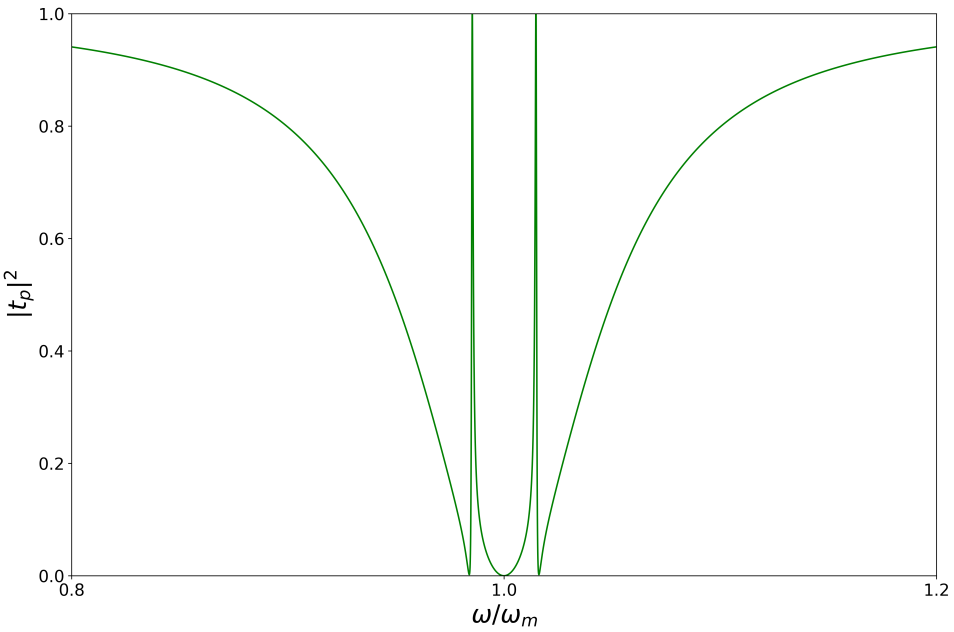

Figure 3.7: Transmission coefficient of probe for mechanical coupling $\mu = 1.5(\gamma + \gamma')$. Other parameters are same as Figure 3.4.

Double OMIT can also be obtained by coupling a mechanical resonator to two-level system. Coupling between mechanical resonator and two-level system results in two dressed states and system becomes a four-level system [32]. Furthermore, two coupled $\mathcal{PT}$ symmetric cavities and two coupled mechanical resonators with Coloumb interaction create double OMIT and double optomechanically induced absorption (OMIA) depending on parameters [83]. Transition from single OMIT, OMIA to double windows is achieved by modulating the Coloumb interaction between mechanical resonators. Coloumb coupling and gain rate of the first cavity (active one) is zero, there will be a absorption window (constructive interference). With the increasing coupling, splitting in absorption and transmission windows occurs and absorption rate enhances in $\mathcal{PT}$ broken phase contrary to our case in which transmission window enhances in unbroken phase [83]. Width between the transparency windows is the frequency difference between dressed states. As can be seen from Figure 3.7, this width becomes larger with increasing coupling constant since $\omega_\pm$ grows. Up conversion process of control field leads to double OMIT seen in Figure 3.6 and Figure 3.7 [27].

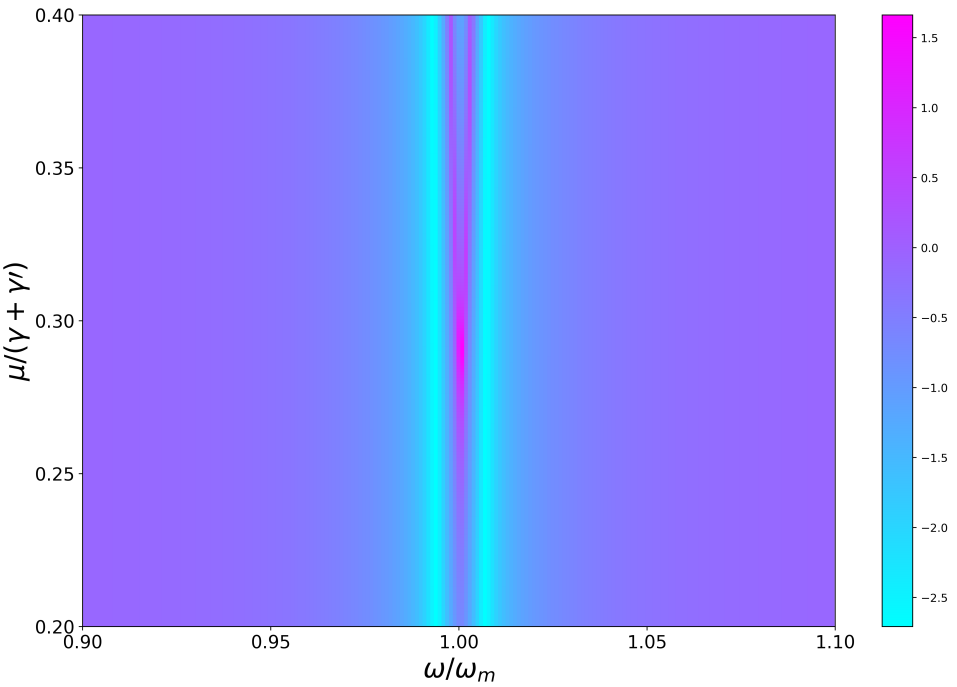

Figure 3.8: The logarithm of transmission coefficient of probe with respect to coupling constant μ and probe detuning ω. Other parameters are same as Figure 3.4.

From Figure 3.8, enhancement of maximum value of transmission probability at $\omega = \omega_m$ around EP is seen where $\mu/(\gamma+\gamma')$ corresponds to 0.30 . Furthermore, transition from single to double OMIT when passing through the EP i.e phase transition is observed clearly from branch and this transition can be modified with the EP. System exhibits a strong dependence on mechanical coupling constant, as the width of transparency windows increase with μ as well as the enhancement of maximum value around EP.

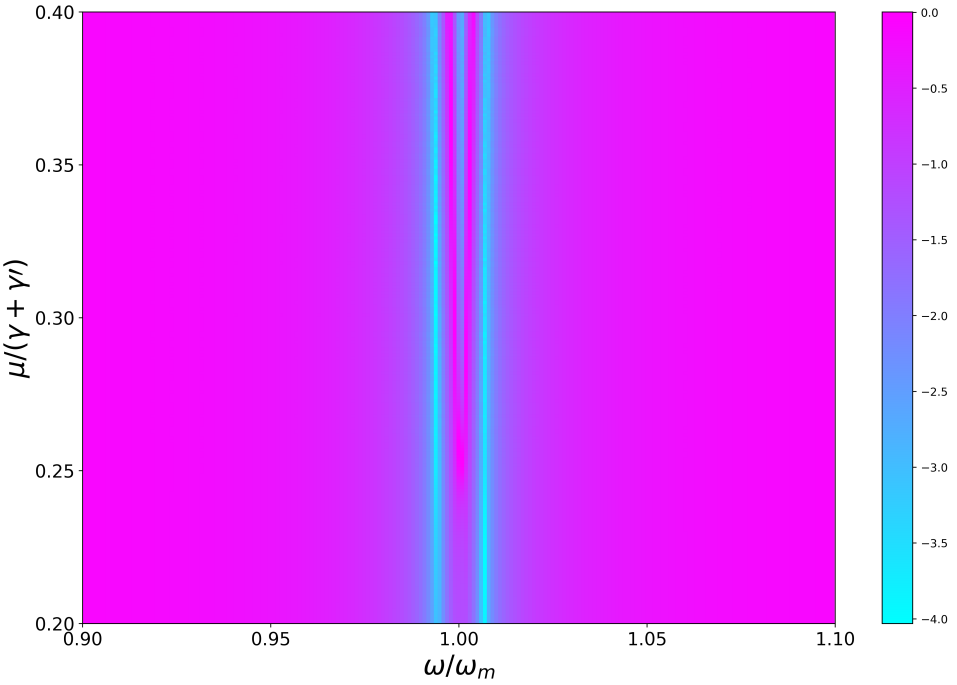

Figure 3.9: The logarithm of transmission coefficient of probe with respect to coupling constant μ and probe detuning ω for polaron transformation approach. Other parameters are same as Figure 3.4.

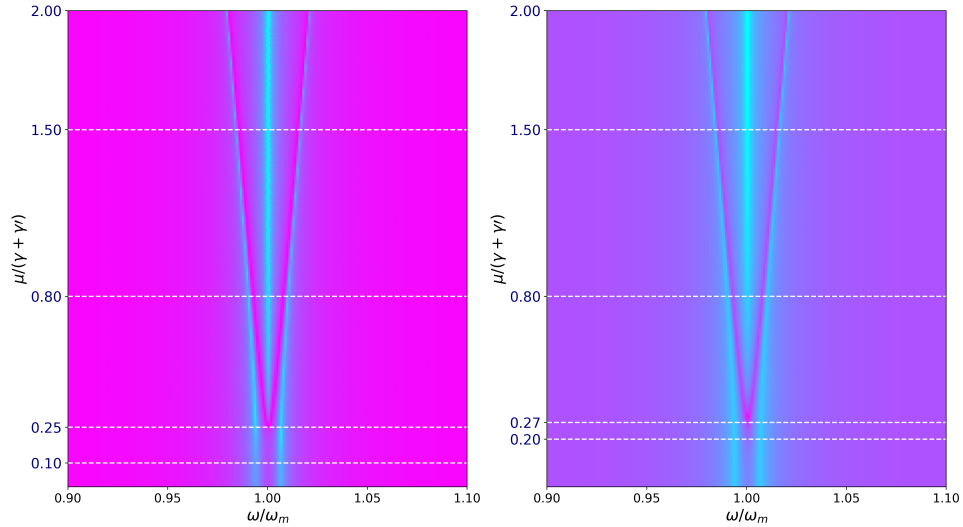

Figure 3.10: Logarithm of power probe transmission for two approaches, white dashed lines are corresponding coupling values for other figures. Plot on the left is for the polaron transformation.

Polaron transformation demonstrates more sensitivity to mechanical coupling constant and as it is seen in Figure 3.9 transition from single OMIT to double OMIT appears earlier than the previous approach. This is the reason of weaker enhancement of peak contrary to first case. If values for μ are chosen as previous cases the transition to double OMIT and enhancement of the maximum value can not be observed properly. For previous case, double windows start to appear around $\mu/(\gamma+\gamma') = 0.31$ and enhancement is observed around $\mu/(\gamma+\gamma') = 0.27$ where EP is at 0.25. However, for current case double windows appear around 0.27 which is very close to EP and enhancement point of previous approach. Based on this graph and deductions, values for μ are chosen as $0.1(\gamma+\gamma')$, $0.25(\gamma+\gamma')$, $0.8(\gamma+\gamma')$, $1.5(\gamma+\gamma')$. More pronounced demonstration of this sensitivity is seen in Figure 3.10.

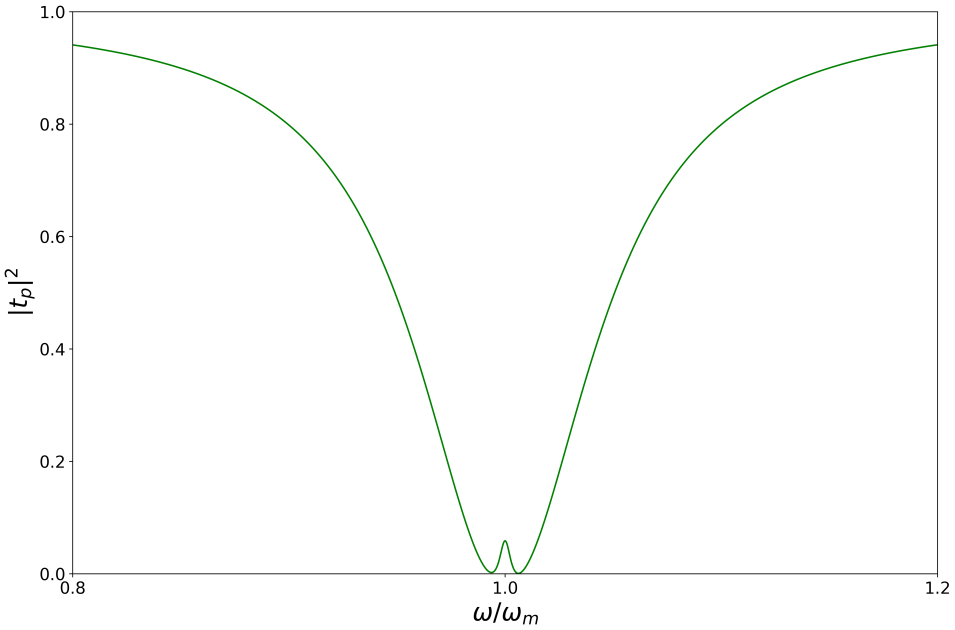

Figure 3.11: Transmission coefficient of probe for mechanical coupling constant $\mu = 0.1(\gamma+\gamma')$. Other parameters are same as Figure 3.4.

When Figure 3.11 is plotted with $0.2(\gamma+\gamma')$, at the maximum value of transparency window at $\omega = \omega_m$, a branch appears due to the slight formation of double omit, but for this value of coupling constant, window occurs properly. However, there is a difference between Figure 3.11 and Figure 3.5, maximum

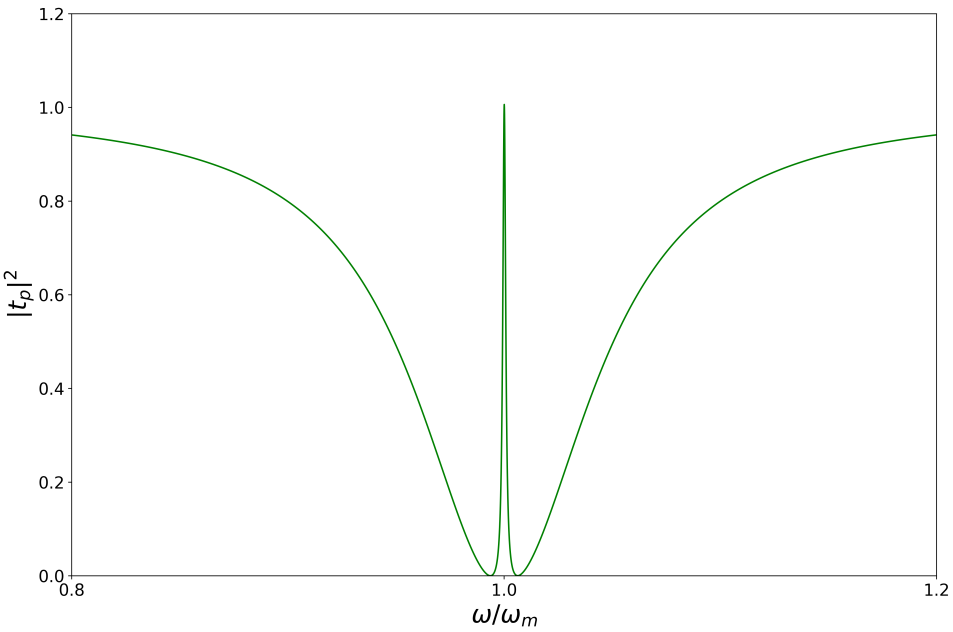

Figure 3.12: Transmission coefficient of probe for mechanical coupling constant $\mu = 0.25(\gamma + \gamma')$. Other parameters are same as Figure 3.4.

value of transparency windows are different. Figure 3.11's peak value is larger than this one.

Figure 3.12 is plotted exactly at EP and an enhancement appears with respect to previous figure. Maximum value becomes nearly twelve times of Figure 3.11. Nevertheless, for previous approach enhancement is much larger than this one, maximum value goes near 5 in y-axis. When system undergoes a phase transition, exactly after the EP double OMIT appears slightly for this approach contrary to Ref. [27] since even in the unbroken phase double OMIT does not appear immediately but in broken phase dressed states are formed due to the nondegenerate supermode frequencies.

As for Figure 3.13 and Figure 3.14, double OMIT occurs and the width between windows becomes larger with increasing μ which is no different than the previous approach and also the values are same for coupling constant. In addition, although there is an enhancement of maximum value of windows first single transparency windows around EP with increasing coupling value, for double transparency windows this is not the case. With increasing coupling value

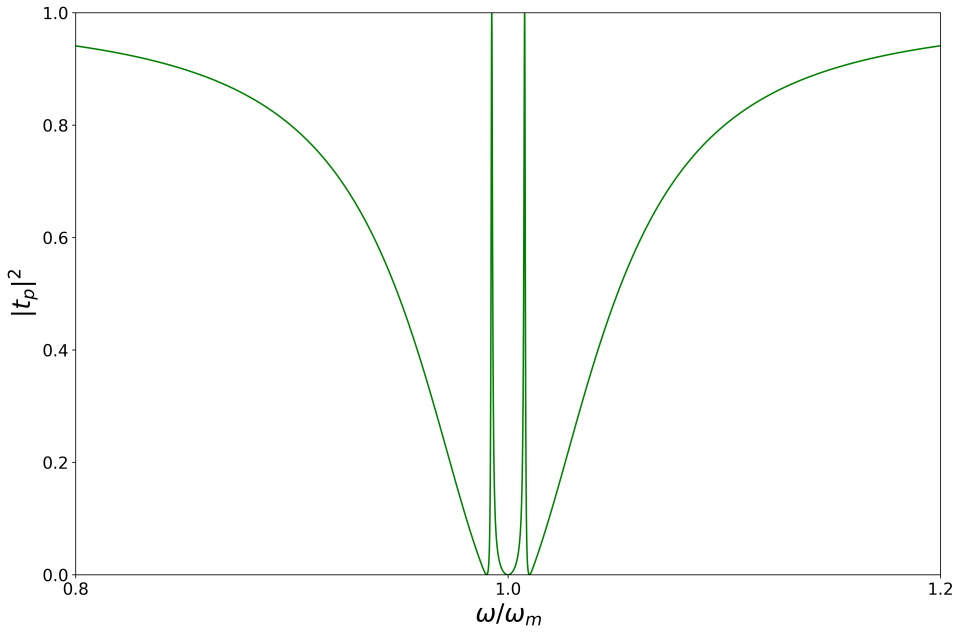

Figure 3.13: Transmission coefficient of probe for mechanical coupling constant $\mu = 0.8(\gamma + \gamma')$. Other parameters are same as Figure 3.4.

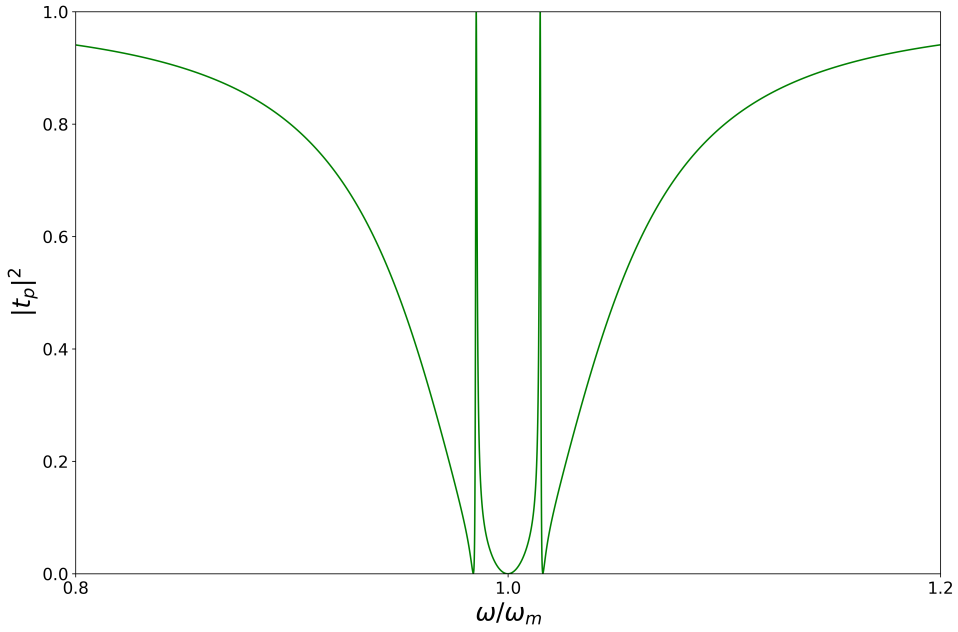

Figure 3.14: Transmission coefficient of probe for mechanical coupling constant $\mu = 1.5(\gamma + \gamma')$. Other parameters are same as Figure 3.4.

linewidth between windows increases but the peak values do not increase for both cases.

3.10 Slow and Fast Light Transmission of the Probe

Before proceeding to slow light transition, given parameters must be discussed. Amplitude of control laser (ε_l) is not supplied in Ref. [27], but only power of control field is given, and the amplitude which is found using the power and wavelength of control field does not produce the current results. After testing for different parameter sets, we deduced that plots in Ref. [27] are closely reproduced for $\varepsilon_l = 0.5$. Accuracy of the present amplitude is confirmed after obtaining similar results with polaron transformation using the same parameter set.

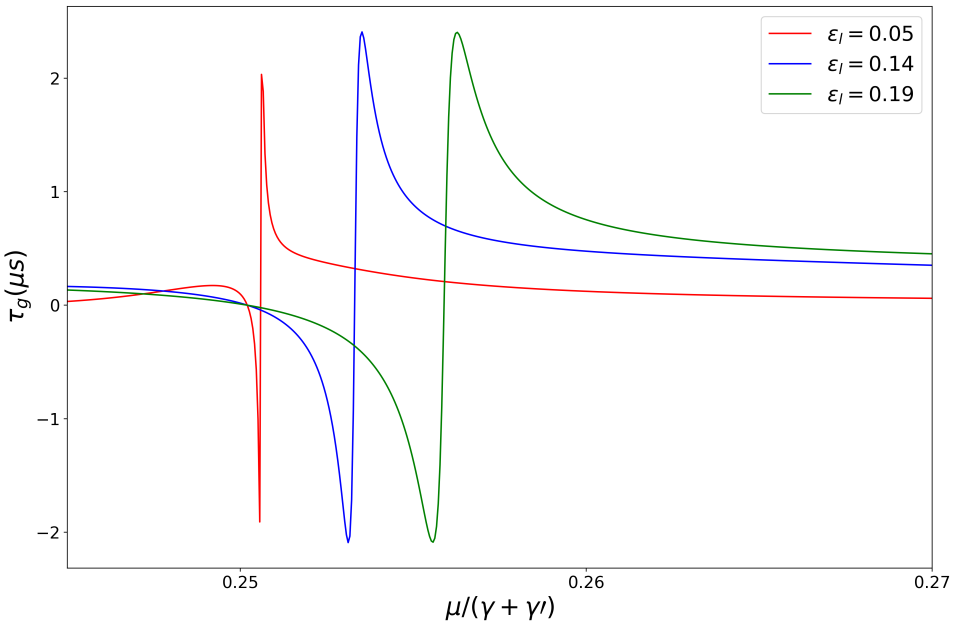

Figure 3.15: Group delay τ_g of probe light with respect to coupling parameter μ where detuning of probe is ω_m.

Moreover, there is another point that needs to be emphasized in Ref. [27].

The authors mention that slow-fast light transition occurs for small control powers and even with such small powers, light can be manipulated and transition can be observed. Unfortunately, we cannot make a comparison for the control power due to the ambiguity of given parameters in Ref. [27]. According to amplitudes that give fast to slow light transition, at least we can say that difference between these three powers (see Figure 3.15) is higher than the one in Ref. [27]. Figure 3.15 demonstrates the relationship between power of the control field and slow light. Transition to slow light occurs at the EP and this transition shifts to $\mathcal{PT}$ unbroken phase with increasing control power. In Ref. [27], this is interpreted as the manipulation of slow light with the control of EP. However, there is not any explained relationship between P_c and the EP.

Chapter 4

Optomechanically Induced Transparency in Ternary Coupled $\mathcal{PT}$ Symmetric System

4.1 Introduction

In this chapter, we discuss the effects of ternary coupling between cavity and the two mechanical resonators on OMIT where most of the system parameters are the same as Chapter 3. As a (notational) change, we have $\gamma = \gamma_1$, $\gamma' = -\gamma_2$, $g = g_1$, and g_2 is the third coupling between second resonator and cavity whereas in the previous chapter cavity was coupled only to passive mechanical resonator (see Figure 4.1). In other words, when $g_2 = 0$, system reduces to Ref. [27]. For simplicity, we assume that both mechanical resonators oscillate with same frequency ω_m. However, coupling coefficients are different, and our specific aim here is to observe phase relationships between g_1 and g_2 where $g_2 = |g_2|e^{i\phi_2}$ and $g_1, \mu \in \mathbb{R}$.

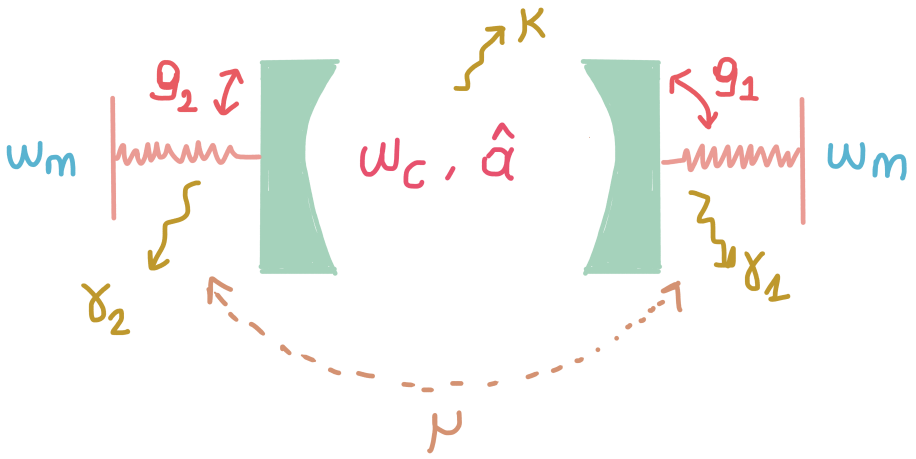

Figure 4.1: Schematic diagram of ternary coupled $\mathcal{PT}$ symmetric optomechanical system with a cavity coupled to two mechanical resonators from both ends.

4.2 Formulation

Hamiltonian is

$$\begin{aligned}\hat{H} =&\hbar\Delta\hat{a}^\dagger\hat{a} + \hbar\omega_m(\hat{b}_1^\dagger\hat{b}_1 + \hat{b}_2^\dagger\hat{b}_2) - \hbar(\mu\hat{b}_1^\dagger\hat{b}_2 + \mu^*\hat{b}_2^\dagger\hat{b}_1) - \hbar\hat{a}^\dagger\hat{a}(g_1\hat{b}_1^\dagger + g_1^*\hat{b}_1)\\ &- \hbar\hat{a}^\dagger\hat{a}(g_2\hat{b}_2^\dagger + g_2^*\hat{b}_2) + i\hbar\sqrt{\eta\kappa}\varepsilon_l(\hat{a}^\dagger - \hat{a}) + i\hbar\sqrt{\eta\kappa}\varepsilon_p(\hat{a}^\dagger e^{-i\omega t} - \hat{a}e^{i\omega t}).\end{aligned} \tag{4.1}$$

Heisenberg-Langevin equations are

$$\begin{aligned}\frac{d\hat{a}}{dt} &= -i\Delta\hat{a} + i\hat{a}(g_1\hat{b}_1^\dagger + g_1^*\hat{b}_1) + i\hat{a}(g_2\hat{b}_2^\dagger + g_2^*\hat{b}_2) + \sqrt{\eta\kappa}\epsilon_l + \sqrt{\eta\kappa}\varepsilon_p e^{-i\omega t} - \frac{\kappa}{2}\hat{a},\\ \frac{d\hat{b}_1}{dt} &= -i\omega_m\hat{b}_1 + i\mu\hat{b}_2 + ig_1\hat{a}^\dagger\hat{a} - \frac{\gamma_1}{2}\hat{b}_1,\\ \frac{d\hat{b}_2}{dt} &= -i\omega_m\hat{b}_2 + i\mu^*\hat{b}_1 + ig_2\hat{a}^\dagger\hat{a} - \frac{\gamma_2}{2}\hat{b}_2.\end{aligned} \tag{4.2}$$

From HL equations, steady state solutions for photon and phonon modes are found as

$$\begin{aligned}\bar{a} &= \frac{\sqrt{\eta\kappa}\varepsilon_l}{i\Delta + \frac{\kappa}{2} - i(g_1\bar{b}_1^* + g_1^*\bar{b}_1) - i(g_2\bar{b}_2^* + g_2^*\bar{b}_2)},\\ \bar{b}_1 &= \frac{ig_1(i\omega_m + \gamma_2/2)|\bar{a}|^2 - \mu g_2|\bar{a}|^2}{(i\omega_m + \gamma_1/2)(i\omega_m + \gamma_2/2) + |\mu|^2},\\ \bar{b}_2 &= \frac{ig_2|\bar{a}|^2 + i\mu^*\bar{b}_1}{i\omega_m + \gamma_2/2}.\end{aligned} \tag{4.3}$$

Evolution equations of perturbation terms are

$$\begin{aligned}
\frac{d\delta\hat{a}}{dt} =& -i\Delta\delta\hat{a} - \frac{\kappa}{2}\delta\hat{a} + i\delta\hat{a}(g_1\bar{b}_1^* + g_1^*\bar{b}_1) + i\bar{a}(g_1\delta\hat{b}_1^* + g_1^*\delta\hat{b}_1) \\
&+ i\delta\hat{a}(g_2\bar{b}_2^* + g_2^*\bar{b}_2) + i\bar{a}(g_2\delta\hat{b}_2^* + g_2^*\delta\hat{b}_2) + \sqrt{\eta\kappa}\varepsilon_p e^{-i\omega t}, \\
\frac{d\delta\hat{b}_1}{dt} =& -i\omega_m\delta\hat{b}_1 - \frac{\gamma_1}{2}\delta\hat{b}_1 + ig_1(\bar{a}\delta\hat{a}^* + \bar{a}^*\delta a) + i\mu\delta\hat{b}_2, \\
\frac{d\delta\hat{b}_2}{dt} =& -i\omega_m\delta b_2 - \frac{\gamma_2}{2}\delta\hat{b}_2 + ig_2(\bar{a}\delta\hat{b}^* + \bar{a}^*\delta\hat{b}) + i\mu^*\delta\hat{b}_1.
\end{aligned} \tag{4.4}$$

Amplitude of anti-Stokes field and transmission of the probe field are

$$\begin{aligned}
A_{1-} &= \frac{\sqrt{\eta\kappa}\varepsilon_p}{\Xi(\omega) - |\bar{a}|^2\Lambda(1-\Gamma)}, \\
t_p &= 1 - \frac{\eta\kappa}{\Xi(\omega) - |\bar{a}|^2\Lambda(1-\Gamma)},
\end{aligned} \tag{4.5}$$

where

$$\begin{aligned}
&\Xi(\omega) = i\Delta + \kappa/2 - i\omega - i(g_1\bar{b}_1^* + g_1^*\bar{b}_1) - i(g_2\bar{b}_2^* + g_2^*\bar{b}_2), \\
&\alpha_1(\omega_m) = -i\omega - i\omega_m + \frac{\gamma_1}{2}, \\
&\alpha_2(\omega_m) = -i\omega - i\omega_m + \frac{\gamma_2}{2}, \\
&f_1(\alpha_1,\alpha_2) = \alpha_1(-\omega_m)\alpha_2(-\omega_m) + |\mu|^2, \\
&f_2(\alpha_1,\alpha_2) = \alpha_1(\omega_m)\alpha_2(\omega_m) + |\mu|^2, \\
&\Lambda = ig_1\left(\frac{-ig_1^*\alpha_2(\omega_m) - \mu^* g_2^*}{f_2(\alpha_1,\alpha_2)}\right) + ig_1^*\left(\frac{ig_1\alpha_2(-\omega_m) - \mu g_2)}{f_1(\alpha_1,\alpha_2)}\right) \\
&+ ig_2\left(\frac{-ig_2^*\alpha_1(\omega_m) - \mu g_1^*}{f_2(\alpha_1,\alpha_2)}\right) + ig_2^*\left(\frac{ig_2\alpha_1(-\omega_m) - \mu^* g_1)}{f_1(\alpha_1,\alpha_2)}\right), \\
&\Gamma = \frac{|\bar{a}|^2\Lambda}{(\Xi(-\omega))^* + \Lambda|\bar{a}|^2}.
\end{aligned} \tag{4.6}$$

As a check, when $g_2 = 0$ all equations reduce to those in Chapter 3.

4.3 Results

Figure 4.2 illustrates the behaviour of double OMIT in ternary coupled optomechanical system for four different phases, ϕ_2. In part (a), which is two coupling

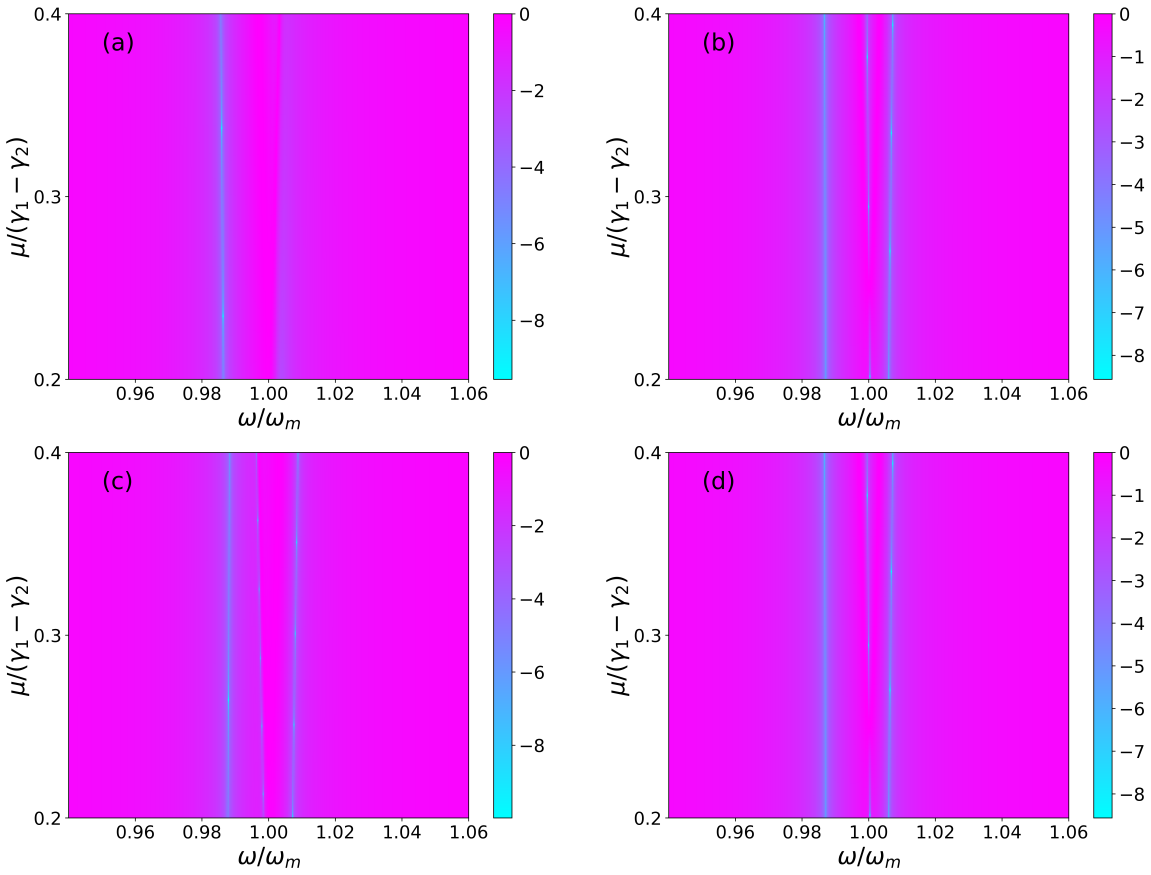

Figure 4.2: Logarithm of transmission coefficient with respect to mechanical coupling and probe detuning for different phase values. Phase values for (a)-(d) are 0, $\pi/2$, π, $3\pi/2$ respectively where modulus of g_2 is equal to g_1. Other parameters are same as in Figure 3.4.

constants are in phase and equal in magnitude, double OMIT tends to disappear. Also, for part (c) which is $\phi_2 = \pi$ i.e $g_2 = -g_1$, double OMIT again cannot be observed, and the symmetry in double OMIT is broken but this time since sign of second coupling changes so that higher peak point in probe transmission shifts to lower branch. When probe detuning is equal to mechanical frequency probe transmission will not be zero in $\mathcal{PT}$ unbroken phase. For part (b) and (d), symmetry is broken but double OMIT occurs at the EP.

Figure 4.3 and Figure 4.4 demonstrate the effect of phase on power probe transmission. For Figure 4.3, in $\mathcal{PT}$ broken phase, $|g_2| = g_1$ affects power probe transmission more than the $|g_2| = 0.3\ g_1$ case. Peak points change dramatically in

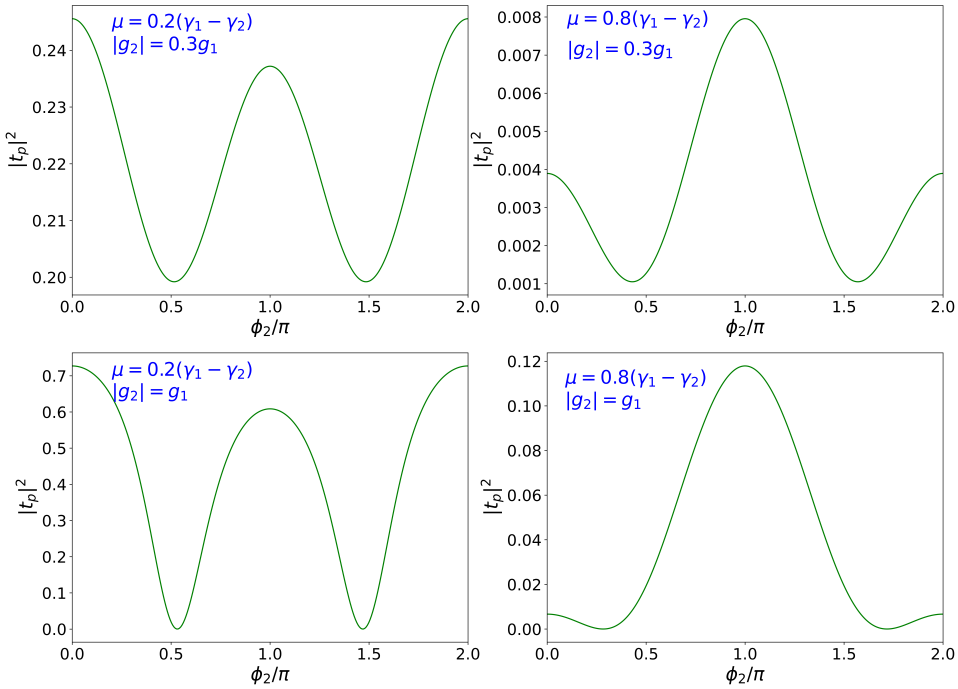

Figure 4.3: Power transmission coefficient versus phase relationship for different μ and $|g_2|$. System parameters are $\omega/\omega_m = 1$, $\mu = 0.2(\gamma_1 - \gamma_2)$, $\mu = 0.8(\gamma_1 - \gamma_2)$ and $|g_2| = 0.3g_1$, $|g_2| = g_1$. Other parameters stay same as in Figure 3.4.

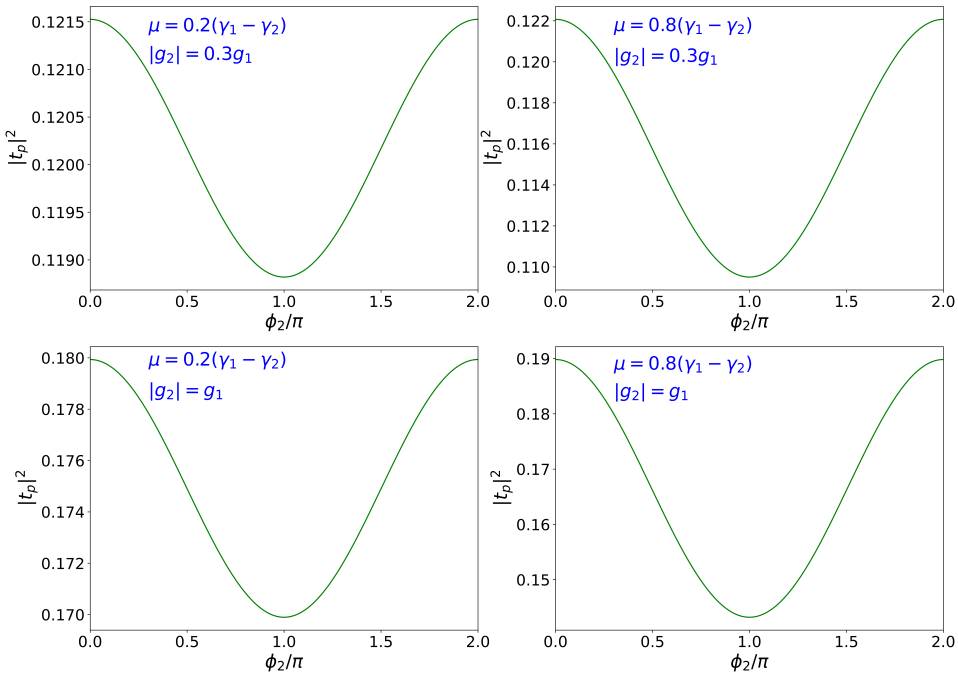

Figure 4.4: Power transmission coefficient versus phase relationship for different μ and $|g_2|$ where $\omega/\omega_m = 1.02$. Other parameters stay same as in Figure 4.3

$|g_2| = g_1$ case. More generally, imaginary coupling constants leads to decrease in power probe transmission. In $\mathcal{PT}$ unbroken phase, probe transmission decreases with increasing modulus of g_2 slightly. For $\omega = 1.02\ \omega_m$, there is no dramatic change like in the Figure 4.3. However, the effect of phase relationship is the opposite of Figure 4.3, when phase is $\phi_2 = \pi$ power probe transmission decreases in contrast to Figure 4.3. Our results for this ternary system are rather preliminary, and there remains more to be done, as will be highlighted in our Conclusion chapter.

Chapter 5

Conclusion

This thesis aims to present detailed formulations as well as the analysis of a $\mathcal{PT}$ symmetric optomechanical system in regard to OMIT. The system consists of a cavity coupled to $\mathcal{PT}$ symmetric mechanical resonators. In Chapter 3, as the first approach, we calculated the transmission of the probe field by finding the HL equations and linearizing the equations to be able to obtain EOM for perturbation terms. In $\mathcal{PT}$ broken phase, a transparency window occurs, and around the EP there is a considerable enhancement of maximum value of transparency window. However, in $\mathcal{PT}$ unbroken phase, i.e., at the other side of EP, there is a transition from single to double OMIT and with the increasing mechanical coupling, μ, between mechanical resonators, the width of the two windows becomes larger.

As an alternative, we proposed the polaron transformation approach to compare the results with Ref. [27]. First, we diagonoalized the mechanical Hamiltonian, and applying a polaron transformation, optomechanical Hamiltonian is diagonalized in the absence of external driving fields. We again observed an enhancement in OMIT but in this case, peak value is not as high as the first approach. Moreover, for this approach transition from single to double OMIT arises at exactly EP contrary to previous one.

For the first approach, system displays a transition from fast to slow light at

the EP and with the increasing power of control field, this transition shifts to $\mathcal{PT}$ unbroken phase. However, this does not mean that the transition can be manipulated with EP since there is no relationship between EP and the power of the control field.

In Chapter 4, we extended the optomechanical system, and coupled both ends of cavity to two mechanical resonators with different coupling constants to highlight the effects of phase relationships. When $|g_2| = g_1$, and the phase of g_2, $\phi_2 = 0, \pi$, double OMIT can not be observed and symmetry is broken. However, in cases of $\phi_2 = \pi/2,\ 3\pi/2$ two transparency windows arise. Additionally, when $|g_2| = g_1$, changes in power probe transmission are more notable than the $|g_2| = 0.3\ g_1$ case. Probe power transmission takes its minimum values at $\phi_2 = \pi/2,\ 3\pi/2$, and highest values at $\phi_2 = 0$. For $\omega = 1.02\ \omega_m$, probe transmission takes its minimum value at $\phi = \pi$, but there is not so much sensitivity to mechanical coupling in this case.

Finally, we would like to suggest some possible extensions of this thesis in the form of a wish list. Observing the phase relations for such a system using polaron transformation remains as a future work. Ternary coupling is expected to produce a higher-order EP, and we want to investigate this theoretically as well as the ramifications of the pseudo-Hermiticity. In addition to these, we would like to undertake a steady-state stability and squeezed state analysis by solving Lindblad Master equation where $\kappa, \gamma_1, \gamma_2$ are to be taken as lossy terms. Lastly, starting with a coherent photonic and thermal phononic initial states, we want to explore whether a generation of squeezed state can be intermittently observed through dynamics.

Bibliography

[1] M. Aspelmeyer, T. J. Kippenberg, and F. Marquardt, "Cavity optomechanics," *Reviews of Modern Physics*, vol. 86, p. 1391, 2014.

[2] T. J. Kippenberg and K. J. Vahala, "Cavity opto-mechanics," *Optics Express*, vol. 15, pp. 17172–17205, 2007.

[3] M. Metcalfe, "Applications of cavity optomechanics," *Applied Physics Reviews*, vol. 1, p. 031105, 2014.

[4] P. Meystre, "A short walk through quantum optomechanics," *Annalen der Physik*, vol. 525, pp. 215–233, 2013.

[5] A. Clerk and F. Marquardt, "Basic theory of cavity optomechanics," *Cavity Optomechanics : Nano- and Micromechanical Resonators Interacting with Light*, p. 5, 2014.

[6] F. Marquardt and S. M. Girvin, "Optomechanics (a brief review)," *arXiv preprint arXiv:0905.0566*, 2009.

[7] A. Ashkin and J. Gordon, "Cooling and trapping of atoms by resonance radiation pressure," *Optics Letters*, vol. 4, pp. 161–163, 1979.

[8] T. Hänsch and A. Schawlow, "Cooling of gases by laser radiation," *Optics Communications*, vol. 13, pp. 68–69, 1975.

[9] H. J. Metcalf and P. Van der Straten, *Laser cooling and trapping*. Graduate texts in contemporary physics, Springer, 1999.

[10] V. Braginsky, A. Manukin, and T. M. Yu., "Investigation of dissipative ponderomotive effects of electromagnetic radiation," *Soviet Physics JETP*, vol. 31, pp. 1549–1552, 1970.

[11] A. Dorsel, H. Walther, J. McCullen, P. Meystre, and E. Vignes, "Optical bistability and mirror confinement induced by radiation pressure," *Physical Review Letters*, vol. 51, pp. 1550–1553, 1983.

[12] K. F. Braginsky, V.B., *Quantum Measurement*. Cambridge University Press, 1992.

[13] V. Braginsky, *Measurement of Weak Forces in Physics Experiments*. University of Chicago Press, 1977.

[14] I. Tittonen, G. Breitenbach, T. Kalkbrenner, T. Müller, R. Conradt, S. Schiller, E. Steinsland, N. Blanc, and N. de Rooij, "Interferometric measurements of the position of a macroscopic body: Towards observation of quantum limits," *Physical Review A - Atomic, Molecular, and Optical Physics*, vol. 59, pp. 1038–1044, 1999.

[15] K. Jacobs, I. Tittonen, H. M. Wiseman, and S. Schiller, "Quantum noise in the position measurement of a cavity mirror undergoing brownian motion," *Physical Review A*, vol. 60, pp. 538–547, 1999.

[16] C. Caves, "Quantum-mechanical noise in an interferometer," *Physical Review D*, vol. 23, pp. 1693–1708, 1981.

[17] B. Abbott, R. Abbott, R. Adhikari, S. Anderson, M. Araya, H. Armandula, S. Ballmer, B. Barish, J. Betzwieser, G. Billingsley, E. Black, K. Blackburn, R. Bork, V. Boschi, A. Brooks, K. Cannon, L. Cardenas, C. Cepeda, S. Chatterji, D. Coyne, R. DeSalvo, R. Dupuis, C. Echols, P. Ehrens, E. Espinoza, T. Etzel, D. Fazi, T. Fricke, L. Goggin, E. Gustafson, J. Heefner, A. Ivanov, W. Kells, D. Keppel, P. King, V. Kondrashov, D. Kozak, A. Lazzarini, M. Lei, K. Libbrecht, P. Lindquist, M. Mageswaran, K. Mailand, E. Maros, J. Marx, and McIntyr, "Observation of a kilogram-scale oscillator near its quantum ground state," *New Journal of Physics*, vol. 11, p. 073032, 2009.

[18] T. J. Kippenberg and K. J. Vahala, "Cavity optomechanics: Back-action at the mesoscale," *Science*, vol. 321, p. 1172, 2008.

[19] S. Mancini, V. Man'ko, and P. Tombesi, "Ponderomotive control of quantum macroscopic coherence," *Physical Review A*, vol. 55, p. 3042, 1997.

[20] S. Bose, K. Jacobs, and P. Knight, "Preparation of nonclassical states in cavities with a moving mirror," *Physical Review A*, vol. 56, p. 4175, 1997.

[21] W. Marshall, C. Simon, R. Penrose, and D. Bouwmeester, "Towards quantum superpositions of a mirror," *Physical Review Letters*, vol. 91, p. 130401, 2003.

[22] D. Vitali, S. Gigan, A. Ferreira, H. R. Böhm, P. Tombesi, A. Guerreiro, V. Vedral, A. Zeilinger, and M. Aspelmeyer, "Optomechanical entanglement between a movable mirror and a cavity field," *Physical Review Letters*, vol. 98, p. 30405, 2007.

[23] F. Elste, S. M. Girvin, and A. A. Clerk, "Quantum noise interference and backaction cooling in cavity nanomechanics," *Physical Review Letters*, vol. 102, p. 207209, 2009.

[24] S. Machnes, J. Cerrillo, M. Aspelmeyer, W. Wieczorek, M. B. Plenio, and A. Retzker, "Pulsed laser cooling for cavity optomechanical resonators," *Physical Review Letters*, vol. 108, p. 153601, 2012.

[25] M. R. Vanner, I. Pikovski, G. D. Cole, M. Kim, Č. Brukner, K. Hammerer, G. J. Milburn, and M. Aspelmeyer, "Pulsed quantum optomechanics," *Proceedings of the National Academy of Sciences*, vol. 108, pp. 16182–16187, 2011.

[26] F. Marquardt, J. P. Chen, A. A. Clerk, and S. M. Girvin, "Quantum theory of cavity-assisted sideband cooling of mechanical motion," *Physical Review Letters*, vol. 99, p. 093902, 2007.

[27] B. Wang, Z. X. Liu, C. Kong, H. Xiong, and Y. Wu, "Mechanical exceptional-point-induced transparency and slow light," *Optics Express*, vol. 27, pp. 8069–8080, 2019.

[28] S. Gröblacher, K. Hammerer, M. R. Vanner, and M. Aspelmeyer, "Observation of strong coupling between a micromechanical resonator and an optical cavity field," *Nature*, vol. 460, pp. 724–727, 2009.

[29] A. H. Safavi-Naeini, T. M. Alegre, J. Chan, M. Eichenfield, M. Winger, Q. Lin, J. T. Hill, D. E. Chang, and O. Painter, "Electromagnetically induced transparency and slow light with optomechanics," *Nature*, vol. 472, pp. 69–73, 2011.

[30] D. E. Chang, A. H. Safavi-Naeini, M. Hafezi, and O. Painter, "Slowing and stopping light using an optomechanical crystal array," *New Journal of Physics*, vol. 13, p. 023003, 2011.

[31] S. Huang and G. S. Agarwal, "Normal-mode splitting and antibunching in Stokes and anti-Stokes processes in cavity optomechanics: Radiation-pressure-induced four-wave-mixing cavity optomechanics," *Physical Review A*, vol. 81, p. 033830, 2010.

[32] H. Xiong and Y. Wu, "Fundamentals and applications of optomechanically induced transparency," *Applied Physics Reviews*, vol. 5, p. 031305, 2018.

[33] G. S. Agarwal and S. Huang, "Electromagnetically induced transparency in mechanical effects of light," *Physical Review A*, vol. 81, p. 041803, 2010.

[34] S. Weis, R. Rivière, S. Deléglise, E. Gavartin, O. Arcizet, A. Schliesser, and T. J. Kippenberg, "Optomechanically induced transparency," *Science*, vol. 330, pp. 1520–1523, 2010.

[35] Q. Wu, J. Q. Zhang, J. H. Wu, M. Feng, and Z. M. Zhang, "Tunable multi-channel inverse optomechanically induced transparency and its applications," *Optics Express*, vol. 23, pp. 18534–18547, 2015.

[36] S. Shahidani, M. H. Naderi, and M. Soltanolkotabi, "Control and manipulation of electromagnetically induced transparency in a nonlinear optomechanical system with two movable mirrors," *Physical Review A*, vol. 88, p. 053813, 2013.

[37] H. Wang, X. Gu, Y. X. Liu, A. Miranowicz, and F. Nori, "Optomechanical analog of two-color electromagnetically induced transparency: Photon transmission through an optomechanical device with a two-level system," *Physical Review A*, vol. 90, p. 023817, 2014.

[38] S. Huang and G. S. Agarwal, "Electromagnetically induced transparency from two-phonon processes in quadratically coupled membranes," *Physical Review A*, vol. 83, p. 023823, 2011.

[39] Y. Xiao, Y. F. Yu, and Z. M. Zhang, "Controllable optomechanically induced transparency and ponderomotive squeezing in an optomechanical system assisted by an atomic ensemble," *Optics Express*, vol. 22, pp. 17979–17989, 2014.

[40] W. Z. Jia, L. F. Wei, Y. Li, and Y. X. Liu, "Phase-dependent optical response properties in an optomechanical system by coherently driving the mechanical resonator," *Physical Review A*, vol. 91, p. 043843, 2015.

[41] K. Qu and G. S. Agarwal, "Phonon-mediated electromagnetically induced absorption in hybrid opto-electromechanical systems," *Phyical Review A*, vol. 87, p. 031802, 2013.

[42] Z. X. Liu, B. Wang, C. Kong, L. G. Si, H. Xiong, and Y. Wu, "A proposed method to measure weak magnetic field based on a hybrid optomechanical system," *Scientific Reports*, vol. 7, pp. 1–8, 2017.

[43] J. Q. Zhang, Y. Li, M. Feng, and Y. Xu, "Precision measurement of electrical charge with optomechanically induced transparency," *Physical Review A*, vol. 86, p. 053806, 2012.

[44] Q. Wang, J. Q. Zhang, P. C. Ma, C. M. Yao, and M. Feng, "Precision measurement of the environmental temperature by tunable double optomechanically induced transparency with a squeezed field," *Physical Review A*, vol. 91, p. 063827, 2015.

[45] C. M. Bender and S. Boettcher, "Real spectra in non-Hermitian Hamiltonians having $\mathcal{PT}$ symmetry," *Physical Review Letters*, vol. 80, pp. 5243–5246, 1998.

[46] C. M. Bender, D. C. Brody, and H. F. Jones, "Complex extension of quantum mechanics," *Physical Review Letters*, vol. 89, p. 270401, 2002.

[47] C. M. Bender, "Making sense of non-Hermitian Hamiltonians," *Reports on Progress in Physics*, vol. 70, p. 947, 2007.

[48] P. Dorey, C. Dunning, and R. Tateo, "Spectral equivalences, bethe ansatz equations, and reality properties in $\mathcal{PT}$ symmetric quantum mechanics," *Journal of Physics A: Mathematical and General*, vol. 34, pp. 5679–5704, 2001.

[49] P. Dorey, C. Dunning, and R. Tateo *Czechoslovak journal of physics*, vol. 54, pp. 35–41, 2004.

[50] A. Mostafazadeh, "Pseudo-Hermiticity versus $\mathcal{PT}$ symmetry: The necessary condition for the reality of the spectrum of a non-Hermitian Hamiltonian," *Journal of Mathematical Physics*, vol. 43, pp. 205–214, 2002.

[51] A. Mostafazadeh, "Pseudo-Hermiticity versus $\mathcal{PT}$-symmetry. ii. a complete characterization of non-Hermitian Hamiltonians with a real spectrum," *Journal of Mathematical Physics*, vol. 43, pp. 2814–2816, 2002.

[52] A. Mostafazadeh, "Pseudo-Hermiticity versus $\mathcal{PT}$-symmetry iii: Equivalence of pseudo-Hermiticity and the presence of antilinear symmetries," *Journal of Mathematical Physics*, vol. 43, pp. 3944–3951, 2002.

[53] C. E. Rüter, K. G. Makris, R. El-Ganainy, D. N. Christodoulides, M. Segev, and D. Kip, "Observation of parity–time symmetry in optics," *Nature physics*, vol. 6, no. 3, pp. 192–195, 2010.

[54] Ş. K. Özdemir, S. Rotter, F. Nori, and L. Yang, "Parity–time symmetry and exceptional points in photonics," *Nature Materials*, vol. 18, p. 783, 2019.

[55] L. Feng, R. El-Ganainy, and L. Ge, "Non-Hermitian photonics based on parity–time symmetry," *Nature Photonics*, vol. 11, p. 752, 2017.

[56] R. El-Ganainy, K. Makris, M. Khajavikhan, D. Christodoulides, Z. Musslimani, and S. Rotter, "Non-Hermitian physics and $\mathcal{PT}$ symmetry.," *Nature Physics*, vol. 14, pp. 11–19, 2018.

[57] K. G. Makris, R. El-Ganainy, D. N. Christodoulides, and Z. H. Musslimani, "Beam dynamics in $\mathcal{PT}$ symmetric optical lattices," *Phyical Review Letters*, vol. 100, p. 103904, 2008.

[58] R. El-Ganainy, K. G. Makris, D. N. Christodoulides, and Z. H. Musslimani, "Theory of coupled optical $\mathcal{PT}$-symmetric structures," *Optics Letters*, vol. 32, pp. 2632–2634, 2007.

[59] F. Klauck, L. Teuber, M. Ornigotti, M. Heinrich, S. Scheel, and A. Szameit, "Observation of $\mathcal{PT}$-symmetric quantum interference," *Nature Photonics*, pp. 883–887, 2019.

[60] B. Peng, Ş. K. Özdemir, F. Lei, F. Monifi, M. Gianfreda, G. L. Long, S. Fan, F. Nori, C. M. Bender, and L. Yang, "Parity-time-symmetric whispering-gallery microcavities," *Nature Physics*, vol. 10, pp. 394–398, 2014.

[61] C. Yüce, "Topological phase in a non-Hermitian $\mathcal{PT}$ symmetric system," *Physics Letters A*, vol. 379, pp. 1213–1218, 2015.

[62] C. Yüce, "Edge states at the interface of non-Hermitian systems," *Physical Review A*, vol. 97, p. 042118, 2018.

[63] A. Guo, G. Salamo, D. Duchesne, R. Morandotti, M. Volatier-Ravat, V. Aimez, G. Siviloglou, and D. Christodoulides, "Observation of $\mathcal{PT}$-symmetry breaking in complex optical potentials," *Physical Review Letters*, vol. 103, p. 093902, 2009.

[64] S. Longhi, "$\mathcal{PT}$-symmetric laser absorber," *Physical Review A*, vol. 82, p. 031801, 2010.

[65] Y. D. Chong, L. Ge, and A. D. Stone, "$\mathcal{PT}$-symmetry breaking and laser-absorber modes in optical scattering systems," *Physical Review Letters*, vol. 106, p. 093902, 2011.

[66] L. Feng, Z. J. Wong, R.-M. Ma, Y. Wang, and X. Zhang, "Single-mode laser by parity-time symmetry breaking," *Science*, vol. 346, pp. 972–975, 2014.

[67] H. Hodaei, M. A. Miri, A. U. Hassan, W. Hayenga, M. Heinrich, D. Christodoulides, and M. Khajavikhan, "Parity-time-symmetric coupled microring lasers operating around an exceptional point," *Optics letters*, vol. 40, pp. 4955–4958, 2015.

[68] H. Hodaei, M.-A. Miri, M. Heinrich, D. N. Christodoulides, and M. Khajavikhan, "Parity-time-symmetric microring lasers," *Science*, vol. 346, pp. 975–978, 2014.

[69] H. Jing, Ş. K. Özdemir, H. Lü, and F. Nori, "High-order exceptional points in optomechanics," *Scientific reports*, vol. 7, no. 1, pp. 1–10, 2017.

[70] H. Jing, Ş. K. Özdemir, X. Y. Lü, J. Zhang, L. Yang, and F. Nori, "$\mathcal{PT}$-symmetric phonon laser," *Physical Review Letters*, vol. 113, p. 053604, 2014.

[71] X. Y. Lü, H. Jing, J. Y. Ma, and Y. Wu, "$\mathcal{PT}$-symmetry-breaking chaos in optomechanics," *Physical Review Letters*, vol. 114, p. 253601, 2015.

[72] H. Jing, K. Özdemir, Z. Geng, J. Zhang, X. Y. Lü, B. Peng, L. Yang, and F. Nori, "Optomechanically-induced transparency in parity-time-symmetric microresonators," *Scientific Reports*, vol. 5, p. 9663, 2015.

[73] C. M. Bender, P. E. Dorey, C. Dunning, A. Fring, D. W. Hook, H. F. Jones, S. Kuzhel, G. Lévai, and R. Tateo, *$\mathcal{PT}$ symmetry : in quantum and classical physics*. World Scientific Publishing, 2019.

[74] M. V. Berry, "Physics of nonhermitian degeneracies," *Czechoslovak journal of physics*, vol. 54, pp. 1039–1047, 2004.

[75] C. M. Bender, "$\mathcal{PT}$-symmetric quantum theory," *Journal of Physics: Conference Series*, vol. 631, p. 012002, 2015.

[76] Y. Wu, W. Liu, J. Geng, X. Song, X. Ye, C. K. Duan, X. Rong, and J. Du, "Observation of parity-time symmetry breaking in a single-spin system," *Science*, vol. 364, pp. 878–880, 2019.

[77] C. Y. Ju, A. Miranowicz, G. Y. Chen, and F. Nori, "Non-Hermitian Hamiltonians and no-go theorems in quantum information," *Physical Review A*, vol. 100, p. 062118, 2019.

[78] C. M. Bender, J. Brod, A. Refig, and M. E. Reuter, "The C operator in $\mathcal{PT}$-symmetric quantum theories," *Journal of Physics A: Mathematical and General*, vol. 37, p. 10139, 2004.

[79] M. O. Scully and M. S. Zubairy, *Quantum optics*. Cambridge University Press, 1997.

[80] H. Xiong, L.-G. Si, A.-S. Zheng, X. Yang, and Y. Wu, "Higher-order sidebands in optomechanically induced transparency," *Phys. Rev. A*, vol. 86, p. 013815, 2012.

[81] C. Jiang, Y. Cui, Z. Zhai, H. Yu, X. Li, and G. Chen, "Tunable slow and fast light in parity-time-symmetric optomechanical systems with phonon pump," *Optics Express*, vol. 26, pp. 28834–28847, 2018.

[82] A. Nunnenkamp, K. Børkje, and S. M. Girvin, "Single-photon optomechanics," *Physical review letters*, vol. 107, p. 063602, 2011.

[83] X. Zhang, Y. Guo, Y. Zhou, and X. Yi, "Double optomechanically induced transparency and absorption in parity-time-symmetric optomechanical systems," *Physical Review A*, vol. 98, p. 033832, 2018.